arXiv:1405.7918v1 [math.DS] 30 May 2014

ASYMPTOTICS IN A FAMILY OF LINKED STRIP MAPS

HEATHER REEVE-BLACK & FRANCO VIVALDI

Abstract. We apply round-off to planar rotations, obtaining a one-parameter family of invertible maps of a two-dimensional lattice. As the angle of rotation approaches $\pi/2$, the fourth iterate of the map produces piecewise-rectilinear motion, which develops along the sides of convex polygons.

We characterise the dynamics —which resembles outer billiards of polygons— as the concatenation of so-called strip maps, each providing an elementary perturbation of an underlying integrable system. Significantly, there are orbits which are subject to an arbitrarily large number of these perturbations during a single revolution, resulting in the appearance of a novel discrete-space version of near-integrable Hamiltonian dynamics.

We study the asymptotic regime of the limiting integrable system analytically, and numerically some features of its very rich near-integrable dynamics. We unveil a dichotomy: there is one regime in which the nonlinearity tends to zero, and a second where it doesn't. In the latter case, numerical experiments suggest that the distribution of the periods of orbits is consistent with that of random dynamics; in the former case the fluctuations result in an intricate structure of resonances.

Date: June 2, 2014.

1. Introduction

We study an asymptotic problem of planar rotations subject to round-off, which leads to a family of **linked strip maps** on lattices. These two-dimensional dynamical systems originate from repeated applications of a simple scattering mechanism, which we now describe. We consider a line l on the plane, which acts as a refracting surface for a bundle of incoming parallel rays. As the rays cross the surface, they change direction while remaining parallel. The dynamics is provided by a piecewise-constant velocity field $\mathbf{v}$ which assumes the values $\mathbf{v}_1$ and $\mathbf{v}_2$ on the two half-planes determined by l (see figure 1, left). We stipulate, say, that $\mathbf{v}(z) = \mathbf{v}_1$ on l. The components of the vector field must agree in orientation: if $\mathbf{n}$ is any normal to l, we require the scalar products $\mathbf{v}_1 \cdot \mathbf{n}$ and $\mathbf{v}_2 \cdot \mathbf{n}$ to be non-zero and agree in sign. The orbits of the flow $\dot{z} = \mathbf{v}(z)$ are parallel rays joined at l.

Next we perturb the flow by turning it into a map:

$$F_\lambda : \mathbb{R}^2 \to \mathbb{R}^2 \qquad F_\lambda(z) = z + \lambda \mathbf{v}(z), \tag{1}$$

where $\lambda > 0$ is the perturbation parameter. The map F_λ is area-preserving, and it agrees with the time-λ advance map of the flow, except on the strip Σ bounded by l (included) and $F_\lambda^{-1}(l)$ (excluded). Upon crossing the line l, an orbit of F_λ will jump from an orbit of the flow to a nearby orbit, which we interpret as a perturbation of the original motion (figure 1, right). If d is the distance between z and l along the incoming field $\mathbf{v}_1$, then the resulting perturbation is determined solely by the remainder of d modulo $\|\lambda \mathbf{v}_1\|$. The map F_λ is invertible precisely when the orthogonal component of the incoming field is the same as that of the outgoing field; we assume that this transversality condition holds. By varying the parameter λ, we can adjust the width of Σ, hence the size of the perturbation. Variants of this construction will be considered later.

To obtain non-trivial dynamics, we need repeated scattering. We consider a (finite or infinite) sequence $(l_1, l_2, \ldots)$ of lines, rays, and segments which partition the plane into convex domains. We assume that on each domain there is a constant velocity field $\mathbf{v}_j$ and that the fields in any two adjacent domains satisfy the transversality conditions stated above. Then we have a flow defined over $\mathbb{R}^2$ except at the points where two or more lines l_j intersect. The orbits of the flow are polygonal lines, whose vertices belong to the lines l_j.

As above, we turn the flow into a map F_λ which acts by translation by the vectors $\mathbf{v}_j$. As a result, each line l_j gives rise to an adjacent strip Σ_j, where flow and map disagree. In the regions where strips overlap, the map F_λ may be defined, say, by first ordering the strips and then applying the map of highest ranking. The map sending a point in one strip to the image point in the next strip is straightforward —it only requires the computation of a remainder. So the strip-to-strip transit may be eliminated from the dynamics, and the map F_λ becomes a map on $\bigcup \Sigma_j$, which we call a **linked strip map**.

Now let $\mathbb{V}$ be the smallest $\mathbb{Z}$-module containing all the vectors $\mathbf{v}_j$. Its dimension depends on the rational dependencies among these vectors, and in the simplest nontrivial case we have a two-dimensional lattice. The lattice $\mathbb{V}$ and its translates are invariant under F_λ and we are

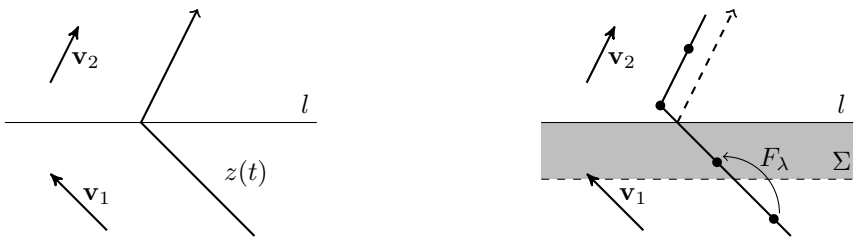

Figure 1. Rays crossing a surface. Left: the flow; right: the map F_λ of equation (1).

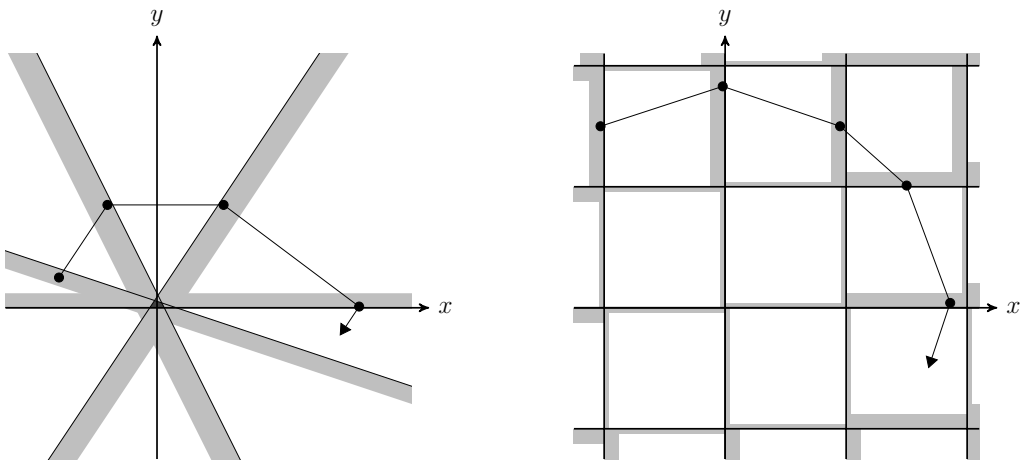

(a) Outer billiard (b) discretised rotations

FIGURE 2. Schematic representation of the linked strip map construction for (a) the outer billiard of a polygon, and (b) the discretised rotation. The latter construction features infinitely many strips.

interested in the restriction of F_λ to these lattices, where the $\lambda \to 0$ scaling of the vector field brings about a highly non-trivial 'quasi-continuum' limit on these lattices.

We consider the case in which the orbits of the flow are closed polygons, which foliate the plane, giving an integrable Hamiltonian system. The map F_λ of equation (1) will be viewed as a perturbation of such an integrable system. Note however, that the transversality condition introduced above is no longer sufficient to guarantee that F_λ is invertible or area-preserving (although it will be so in our case, due to time-reversal symmetry).

Integrable systems with polygonal invariant curves have been studied in the context of ultra-discrete (or tropical) dynamics [Iwa05, Nob08]. Perturbed systems of the linked strip map type appear in outer billiards of convex polygons (see figure 2 (a) and [Tab95]). Here the analogous map is the second iterate of the outer billiard map for all points sufficiently far away from the origin. This coincidence suggests a way of extending the map to the intersection of the strips, which are found near the central polygon. This programme was carried out by Schwartz [Sch11], resulting in the construction of the so-called the *pinwheel map*. Pinwheel maps may be viewed as a generalisation of outer billiard maps, in the sense that the unbounded orbits of the two systems are in one-to-one correspondence.

In this paper we explore a specific invertible linked strip map of a two-dimensional lattice, which results from discretising the space of a one-parameter family of planar rotations via a round-off procedure. The novel feature of this model —to be defined in the next section— is that the number of lines l_j is infinite, and moreover the invariant curves of the underlying integrable system, which are convex polygons, have an arbitrarily large number of sides. When the integrable flow is turned into a map, the orbits located sufficiently far away from the origin meet an arbitrarily large number of strips during a single revolution. This results in a perturbation of increasing complexity—a feature which cannot be achieved in outer billiards of polygons without changing the shape of the billiard. This asymptotic regime is the primary interest of this paper.

1.1. **The model.** The map under study is given by

$$F : \mathbb{Z}^2 \to \mathbb{Z}^2 \qquad F(x, y) = (\lfloor \lambda x \rfloor - y,\, x) \qquad \lambda = 2\cos(2\pi\nu) \tag{2}$$

where $\lfloor \cdot \rfloor$ is the floor function —the largest integer not exceeding its argument. If we remove the floor function in (2), then we obtain a one-parameter family of linear maps of the plane, which,

for $|\lambda| < 2$, are linearly conjugate to a rotation by the angle $2\pi\nu$ (ν is the rotation number). The floor function discretises the space, rounding the image point $(\lambda x - y, x)$ to the nearest lattice point on the left. This map is invertible as well as reversible. (Note that a generic discretised rotation with round-off will not have either property.) In this system the discretisation length is fixed, and the limit of vanishing discretisation corresponds to motions at infinity.

The model (2) has strong arithmetical features. The original motivation for its study came from dynamical systems [Viv94, LHV97, LV98, LV00, BV00, VV03, KLV02]; subsequently, this model was studied in number theory in the area of shift radix systems [ABPT06, ABPS06, ABPS08].

The dynamics of (2) is poorly understood. It has been conjectured that for all real λ with $|\lambda| < 2$ all orbits of F are periodic [ABPT06, Viv06], but this conjecture has been proved for only *eight* values of λ (besides three trivial cases $\lambda = 0, \pm 1$ where the map F is of finite order). These parameters correspond to the rational values of the rotation number ν for which λ is a quadratic irrational [LHV97, KLV02, ABPS08]. The proof relies on an embedding in a two dimensional torus, where the system becomes an exactly renormalisable piecewise isometry, which is a zero-entropy system. The lack of renormalisability for algebraic parameters of degree three or higher has so far prevented further progress.

The map (2) is known to have infinitely many periodic orbits for all parameter values [AP13]; however these orbits have zero density. The analysis of rational λ-values (for which ν is irrational) gives some insight into the difficulties one encounters to establish periodicity. In the simplest scenario, where the denominator of λ is the power of a prime p, the map F admits a dense embedding in the ring $\mathbb{Z}_p$ of p-adic integers. The embedding dynamics has positive entropy, being the composition of an isometry and a full shift [BV00, VV03]. The periodic orbits of the round-off map form a thin subset of all periodic orbits of the embedding system: establishing their properties is predictably difficult.

In this work we consider the limit $\lambda \to 0$, which we refer to as the **integrable limit**. As pointed out above, at $\lambda = 0$ the dynamics is trivial: there is no round-off and the mapping has order four ($\nu = 1/4$). In this parameter regime there is a new natural embedding of F, this time into the plane, and a new dynamical mechanism, namely a discrete-space version of linked strip maps. Some properties of this systems were studied in [RBV13], and we will review them below.

The connection with linked strip maps stems from the fact that, as λ approaches 0, the iterated map F^4 is close to the identity, suggesting the introduction of a *discrete vector field* on the scaled lattice $(\lambda\mathbb{Z})^2$:

$$\mathbf{v}_\lambda(z) = F_\lambda^4(z) - z,$$

where F_λ is a scaled version of (2):

$$F_\lambda : (\lambda\mathbb{Z})^2 \to (\lambda\mathbb{Z})^2 \qquad F_\lambda(z) = \lambda F(z/\lambda) \qquad \lambda > 0. \tag{3}$$

For λ sufficiently close to 0, the module $\mathbb{V}$ of $\mathbf{v}_\lambda$ is $(\lambda\mathbb{Z})^2$. The parameter λ controls not only the rotation number ν, but also the lattice spacing. It turns out that, as $\lambda \to 0$, the field $\mathbf{v}_\lambda$ becomes piecewise-constant, albeit in a non-uniform manner. The domains of rectilinear motion become a regular array of squares, bounded by an infinite array of orthogonal lines l_j.

More precisely, there is an auxiliary integrable Hamiltonian vector field $\mathbf{w}$ on $\mathbb{R}^2$, with the property that, if λ is sufficiently small, then $\lambda\mathbf{w}$ agrees with $\mathbf{v}_\lambda$ over any bounded domain of the plane, apart from regions of negligible total measure. This field is given by:

$$\mathbf{w} : \mathbb{R}^2 \to \mathbb{Z}^2 \qquad \mathbf{w}(x, y) = (2\lfloor y \rfloor + 1, -(2\lfloor x \rfloor + 1)). \tag{4}$$

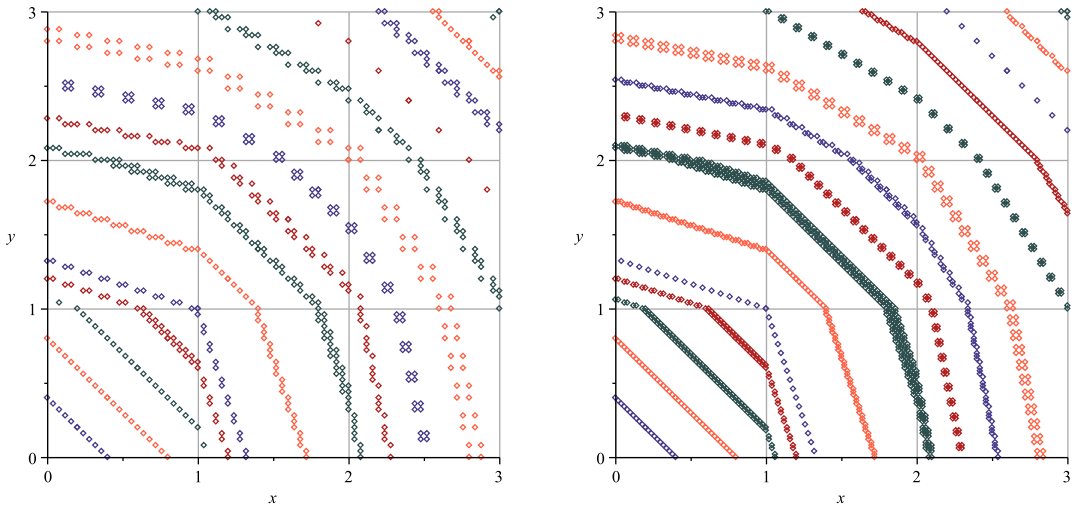

(a) $\lambda = 1/25$ (b) $\lambda = 1/50$

FIGURE 3. Some periodic orbits of the rescaled map F_λ for small values of the parameter λ. The view is restricted to the first quadrant. The lattice spacing is such that each unit distance contains $1/\lambda$ lattice points.

The convex domains on which $\mathbf{w}$ is constant are bounded by the array of orthogonal lines $x = i$ and $y = j$, for integer i, j. These domains are translated unit squares (called **boxes**)

$$B_{m,n} = (m, n) + [0, 1)^2 \qquad m, n \in \mathbb{Z} \tag{5}$$

and the field across adjacent boxes satisfies the transversality condition mentioned above. The module $\mathbb{V}$ of $\mathbf{w}$ is generated by $(1, 1)$ and $(1, -1)$, and hence has index 2 in $\mathbb{Z}^2$. The corresponding Hamiltonian $\mathscr{H}$ is given by

$$\mathscr{H} : \mathbb{R}^2 \to \mathbb{R} \qquad \mathscr{H}(x, y) = P(x) + P(y), \tag{6}$$

where P is the piecewise-affine function

$$P : \mathbb{R} \to \mathbb{R} \qquad P(x) = \lfloor x \rfloor^2 + (2\lfloor x \rfloor + 1)\{x\}, \tag{7}$$

and $\{x\}$ denotes the fractional part of x. The orbits of $\mathscr{H}$ are convex polygons, with an increasing number of sides as one moves away from the origin; near the origin they are squares, while at infinity they approach circles. For small λ, the composite map F_λ^4 is equal to the time-λ advance map of the flow along the edges of the polygons. The perturbation occurs near the vertices, where the orbits are not differentiable.

This structure differs from the pinwheel map in an important respect. Not only is the number of domains over which the field is constant infinite, but in addition, as the distance from the origin increases, the number of components encountered by individual orbits also increases without bounds. In our model the auxiliary vector field $\lambda\mathbf{w}$ is not necessarily equal to the discrete vector field $\mathbf{v}_\lambda$—the two may differ within the strips. This discrepancy —while creating additional complications— admits a simple description.

Thus, in the integrable limit, the rescaled map F_λ is a perturbation of an integrable Hamiltonian system, but the integrable system is no longer a rotation, and the perturbation is no longer caused by round-off. Furthermore, the integrable system is nonlinear, i.e., its time-advance map satisfies a twist condition. When the perturbation is switched on, a discrete-space version of near-integrable Hamiltonian dynamics emerges on the lattice (see figure 3).

1.2. **Outline of the paper & main results.** The study of the rescaled map F_λ at infinity begins with the analysis of the underlying integrable system. The invariant polygons of the Hamiltonian system (6) form countably many foliations, called **polygon classes**. All polygons in a class have the same number of sides, and the classes are indexed by the set $\mathscr{E}$ of natural numbers which can be represented as the sum of two squares:

$$\mathscr{E} = \{e_i \,:\, i \geqslant 0\} = \{0, 1, 2, 4, 5, 8, 9, 10, 13, 16, 17, \dots\}. \tag{8}$$

As $e_i \to \infty$, the corresponding foliation becomes a thin polygonal annulus of approximate radius $\sqrt{e_i}$. Further definitions and results from [RBV13] will be reviewed in section 2.

Then we construct a Poincaré return map for the integrable system. We consider a the time-advance map of the flow and its first return to a thin strip X placed along the symmetry line $x = y$. The width of the strip is equal to the magnitude of the the field $\lambda\mathbf{w}$ and since a point and its translate by $\lambda\mathbf{w}$ are naturally identified, we have a return map of a cylinder. Its behaviour is determined by the period of the flow, which varies in a piecewise-affine manner within each polygon class.

In section 3 we study the return map at infinity. For each class there is a change of coordinates which conjugates the unperturbed return map to a linear twist map on the cylinder. The twist condition depends on the derivative of the period function for that class, and as the distance from the origin increases, this function undergoes damped oscillations. Under a suitable scaling, the period function converges to a continuous function with discontinuous first derivative. This in turn leads to a discontinuity in the asymptotic behaviour of the twist map.

More precisely, in section 3 we shall prove the following result, which appears in the text as two separate theorems.

Theorem (Theorem 3, page 13 & theorem 4, page 16)**.** *Associated with each polygon class, indexed by $e \in \mathscr{E}$, there is a change of coordinates which conjugates the unperturbed return map to the linear twist map T^e, given by*

$$T^e : \mathbb{X} \to \mathbb{X} \qquad T^e(\theta, \rho) = (\theta + \kappa\rho, \rho)\,, \tag{9}$$

where $\mathbb{X}$ is the unit cylinder:

$$\mathbb{X} = \mathbb{S}^1 \times \mathbb{R},$$

and $\kappa = \kappa(e)$ is the twist. Furthermore, as $e \to \infty$, the limiting behaviour of $\kappa(e)$ is singular:

$$\kappa(e) \to \begin{cases} 4 & \{\sqrt{e}\} = 0 \\ 0 & \textit{otherwise.} \end{cases}$$

Typically the twist κ converges to zero, and hence the return map converges (non-uniformly) to the identity. However, for the polygon classes for which e is a perfect squares (a thin subsequence of the sequence (8)), the twist approaches a positive value.

Finally, in section 4, we explore numerically the perturbed dynamics at infinity, tracking exactly long orbits of F using integer arithmetic. We study some features of the first-return map to the strip X. This is now a perturbed twist map on a lattice. The twist condition is given by the theorem above, and the perturbation results from the cumulative effect of a large number of strip maps. In the annuli where the twist $\kappa(e)$ tends to zero, the form of the perturbation is laid bare, and we find delicate resonance structures superimposed to low-amplitude fluctuations (see figure 4). By contrast, where the twist persists the phase portrait is featureless, suggesting a statistical approach.

Thus we consider the distribution of the periods of the periodic orbits. Since our system is reversible, it is the composition of two orientation-reversing involutions. The probabilistic model against which to compare the dynamical data was developed in [RV09], where it was

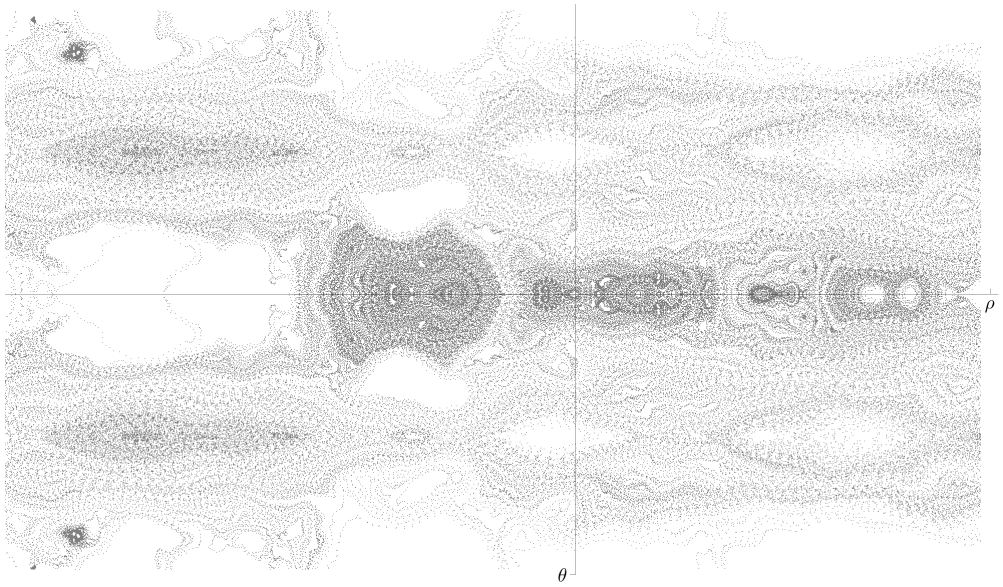

FIGURE 4. A pixel-plot of a primary resonance for $e = 160234 \approx 400.3^2$ and $\lambda \approx 3.5 \times 10^{-9}$. The plot shows part of a large number of symmetric orbits of Φ in the cylindrical coordinates $(\theta, \rho) \in \mathbb{X} = \mathbb{S}^1 \times \mathbb{R}$. The resolution is such that the width of the cylinder consists of approximately 560 lattice sites. There are parts of the cylinder which are filled with symmetric orbits, and others which are devoid of them, but no sharp boundary between the two.

shown that for a suitable scaling of the period, the expected period distribution function of a random reversible map on N points converges pointwise as $N \to \infty$. The limit function is a gamma (or Erlang) distribution

$$\mathcal{R}(x) = 1 - e^{-x}(1 + x). \tag{10}$$

The scaling factor depends on the fraction of the phase space occupied by the fixed sets of the two involutions, see [RV09, Theorem A].

Numerical experiments with various classes of maps over finite fields (polynomial and rational maps of affine and projective spaces and K3 surfaces), which have strong pseudo-random features, have exposed the ubiquity of (10) [RV05, dFH13]. This distribution was subsequently found also for the periodic orbits of a zero-entropy map on lattices [NRV12], suggesting that the emergence of (10) requires only mild statistical properties.

The period distribution function is well-defined in our model, because the return map is equivariant with respect to a group of lattice translations, and so the phase space is a discrete torus. In section 4 we provide numerical evidence that the limit $\mathcal{R}(x)$ is attained along the sub-sequence of polygon classes which correspond to perfect squares, where the nonlinearity of the return map persists at infinity. These findings suggest that a sufficiently large number of linked strip maps can produce a form of 'pseudochaos'.

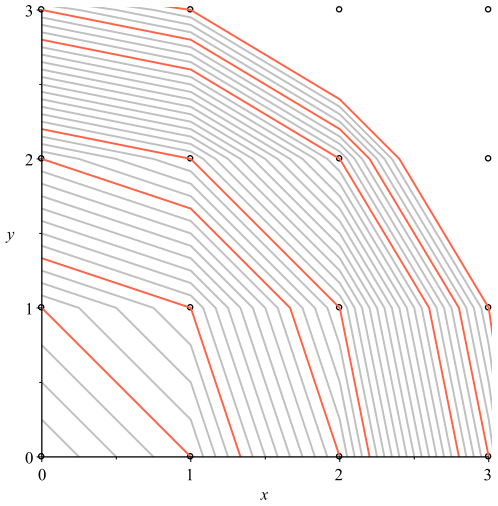

FIGURE 5. A selection of polygons $\mathscr{H}(x,y) = \alpha$ for values of α in the interval $[0, 10]$. The critical polygons are shown in red. The polygon classes are the annuli bounded between pairs of adjacent critical polygons.

2. The integrable flow

We describe the properties of the Hamiltonian $\mathscr{H}$ of equation (6), which was introduced in [RBV13].

The function $\mathscr{H}$ is continuous, piecewise-affine, and differentiable on $\mathbb{R}^2 \setminus \Delta$, where Δ is the set of orthogonal lines given by

$$\Delta = \{(x,y) \in \mathbb{R}^2 \,:\, (x - \lfloor x \rfloor)(y - \lfloor y \rfloor) = 0\}. \tag{11}$$

The corresponding Hamiltonian vector field, wherever it is defined, is equal to the auxiliary vector field $\mathbf{w}$ of equation (4), and is constant on the collection of boxes $B_{m,n}$ of equation (5). The set Δ is the boundary of the boxes $B_{m,n}$. We denote the value of $\mathbf{w}$ on $B_{m,n}$ as

$$\mathbf{w}_{m,n} = (2n+1, -(2m+1)). \tag{12}$$

The orbits —the level sets of $\mathscr{H}$— are **convex polygons** [RBV13, Theorem 2], denoted by

$$\Pi(\alpha) = \{z \in \mathbb{R}^2 \,:\, \mathscr{H}(z) = \alpha\} \qquad \alpha \in \mathbb{R}^+.$$

The vertices of a polygon $\Pi(\alpha)$ occur at its intersections with the set Δ, and all polygons are invariant under the dihedral group D_4, generated by the two orientation-reversing involutions

$$G: \quad (x,y) \mapsto (y,x) \qquad\qquad G': \quad (x,y) \mapsto (x,-y). \tag{13}$$

There is a natural partition of the foliation $\Pi(\alpha)$ into **polygon classes**, separated by **critical polygons**, which contain integer lattice points. Since $\mathscr{H}(x,y) = x^2 + y^2$ whenever x and y are integer, a polygon $\Pi(\alpha)$ is critical precisely when α belongs to the set $\mathscr{E}$ of non-negative integers which are representable as the sum of two squares (see equation (8)), which we call **critical numbers**. The corresponding family of **critical intervals**—the open intervals between consecutive critical numbers—is given by

$$\mathscr{I}^{e_i} = (e_i, e_{i+1}) \qquad e_i \in \mathscr{E}. \tag{14}$$

The critical polygons act as separatrices, delineating a countable set of concentric, open, polygonal annuli, which constitute the polygon classes (see figure 5). We index the polygon classes using the set of critical numbers, and associate the critical number $e \in \mathscr{E}$ with the

polygon class $\mathscr{H}^{-1}(\mathscr{I}^e)$. All polygons in a given class have the same set of edge vectors, i.e., intersect the same collection of boxes $B_{m,n}$.

2.1. **Nonlinearity.** The Hamiltonian $\mathscr{H}$ is nonlinear, since the periods of orbits depend on the initial conditions. We consider the **period function** $\alpha \mapsto \mathscr{T}(\alpha)$, which gives the period of the orbit $\Pi(\alpha)$ as a function of $\alpha > 0$. Adopting the short-hand notation

$$\langle x \rangle := \lfloor \sqrt{x} \rfloor \tag{15}$$

we have the following expression for $\mathscr{T}(\alpha)$.

Proposition 1. *Let $\alpha > 0$. Then the period $\mathscr{T}(\alpha)$ of the Hamiltonian flow on the polygon $\Pi(\alpha)$ is given by*

$$\frac{\mathscr{T}(\alpha)}{8} = \frac{P^{-1}(\alpha/2)}{2\langle \alpha/2 \rangle + 1} - 2 \sum_{n=\langle \alpha/2 \rangle + 1}^{\langle \alpha \rangle} \frac{P^{-1}(\alpha - n^2)}{4n^2 - 1} \tag{16}$$

(where if $\langle \alpha/2 \rangle = \langle \alpha \rangle$ the sum should be understood to be empty).

Note that the function P of equation (7) can only be inverted up to sign, so we write P^{-1} to denote the function

$$P^{-1} : \mathbb{R}_{\geqslant 0} \to \mathbb{R}_{\geqslant 0} \qquad x \mapsto \frac{x + \langle x \rangle (1 + \langle x \rangle)}{2\langle x \rangle + 1}, \tag{17}$$

which satisfies $(P^{-1} \circ P)(x) = |x|$.

Proof. Take $\alpha > 0$. By the eight-fold symmetry of the level sets of $\mathscr{H}$ (see equation (13)), it suffices to consider the intersection of the polygon $\Pi(\alpha)$ with the first octant. The point $(y, y) \in \Pi(\alpha)$ where the polygon intersects the positive half of the symmetry line $\operatorname{Fix} G$ satisfies

$$y = P^{-1}(\alpha/2),$$

whereas the point $(x, 0) \in \Pi(\alpha)$ where the polygon intersects the positive x-axis satisfies

$$x = P^{-1}(\alpha).$$

We consider the time taken to flow between these two points.

From the piecewise-affine form of the function P, it is straightforward to show that

$$\langle x \rangle = \lfloor P^{-1}(x) \rfloor \qquad x \in \mathbb{R}^+, \tag{18}$$

so that by the definition of x and y:

$$\lfloor y \rfloor = \langle \alpha/2 \rangle \qquad \lfloor x \rfloor = \langle \alpha \rangle.$$

To proceed, we partition the y-distance between the two points (y, y) and $(x, 0)$ into a sequence of distances $d(n)$, and corresponding flow-times $t(n)$, for $n = \langle \alpha/2 \rangle, \ldots, \langle \alpha \rangle$. If $\langle \alpha \rangle = \langle \alpha/2 \rangle$ the partition consists of a single element: we simply let $d(\langle \alpha/2 \rangle) = P^{-1}(\alpha/2)$, and $t(\langle \alpha/2 \rangle)$ is the time taken for the flow on $\Pi(\alpha)$ to move between the symmetry lines $x = y$ and $y = 0$.

Suppose now that $\langle \alpha/2 \rangle < \langle \alpha \rangle$. Note that the y-coordinate of the vertex of $\Pi(\alpha)$ which lies in the first octant and has x-coordinate $x = n$ is given by

$$P^{-1}(\alpha - n^2).$$

(Such vertices do not exist if $\langle \alpha \rangle = \langle \alpha/2 \rangle$.) Then we let $d(\langle \alpha \rangle)$ denote the y-distance between the points where $\Pi(\alpha)$ intersects the symmetry line $x = y$ and the line $x = \langle \alpha/2 \rangle + 1$:

$$d(\langle \alpha/2 \rangle) = P^{-1}(\alpha/2) - P^{-1}(\alpha - (\langle \alpha/2 \rangle + 1)^2),$$

and $d(\langle \alpha \rangle)$ denote the y-distance between the points where $\Pi(\alpha)$ intersects the line $x = \langle \alpha \rangle$ and the symmetry line $y = 0$:

$$d(\langle \alpha \rangle) = P^{-1}(\alpha - \langle \alpha \rangle^2).$$

For any n with $\langle\alpha/2\rangle + 1 \leqslant n \leqslant \langle\alpha\rangle - 1$, $d(n)$ is the y-distance between the points where $\Pi(\alpha)$ intersects the lines $x = n$ and $x = n + 1$:

$$d(n) = P^{-1}(\alpha - n^2) - P^{-1}(\alpha - (n+1)^2).$$

Similarly, $t(\langle\alpha/2\rangle)$ is the time taken for the flow on $\Pi(\alpha)$ to move between the symmetry line $x = y$ and $x = \langle\alpha/2\rangle + 1$, $t(\langle\alpha/2\rangle)$ is the time taken to move between the line $x = \langle\alpha\rangle$ and the symmetry line $y = 0$, and for $\langle\alpha/2\rangle + 1 \leqslant n \leqslant \langle\alpha\rangle - 1$, $t(n)$ is the time taken to flow between the lines $x = n$ and $x = n + 1$.

With this notation, and using the symmetry of the flow (13), the period $\mathscr{T}(\alpha)$ satisfies

$$\frac{\mathscr{T}(\alpha)}{8} = \sum_{n=\langle\alpha/2\rangle}^{\langle\alpha\rangle} t(n). \tag{19}$$

For any $n \geqslant 0$, the auxiliary vector field has constant y-component between the lines $x = n$ and $x = n + 1$, given by $-(2n + 1)$ (see equation (4)). Hence the times $t(n)$ and the distances $d(n)$ are related by

$$t(n) = \frac{d(n)}{2n+1} \qquad \langle\alpha/2\rangle \leqslant n \leqslant \langle\alpha\rangle. \tag{20}$$

If $\langle\alpha/2\rangle = \langle\alpha\rangle$ then the result follows from the definition of $d(\langle\alpha/2\rangle)$. If $\langle\alpha/2\rangle < \langle\alpha\rangle$, substituting (20) and the definition of the $d(n)$ into (19) gives:

$$\begin{aligned}
\frac{\mathscr{T}(\alpha)}{8} &= \sum_{n=\langle\alpha/2\rangle}^{\langle\alpha\rangle} \frac{d(n)}{2n+1} \\
&= \frac{P^{-1}(\alpha/2)}{2\langle\alpha/2\rangle + 1} + \sum_{n=\langle\alpha/2\rangle+1}^{\langle\alpha\rangle} \frac{P^{-1}(\alpha - n^2)}{2n+1} - \sum_{n=\langle\alpha/2\rangle}^{\langle\alpha\rangle-1} \frac{P^{-1}(\alpha - (n+1)^2)}{2n+1} \\
&= \frac{P^{-1}(\alpha/2)}{2\langle\alpha/2\rangle + 1} - 2 \sum_{n=\langle\alpha/2\rangle+1}^{\langle\alpha\rangle} \frac{P^{-1}(\alpha - n^2)}{4n^2 - 1},
\end{aligned}$$

as required. □

Now we consider the derivative of the period function $\mathscr{T}$. If the derivative is non-zero, then the flow is nonlinear.

Proposition 2. *Let $e \in \mathscr{E}$ be a critical number and let $\alpha \in \mathscr{I}^e$ be some value in the critical interval associated with e. Then the derivative $\mathscr{T}'(\alpha)$ of the period of the Hamiltonian flow on the polygon $\Pi(\alpha)$ is given by*

$$\frac{\mathscr{T}'(\alpha)}{4} = \frac{1}{(2\langle e/2\rangle + 1)^2} - 4 \sum_{n=\langle e/2\rangle+1}^{\langle e\rangle} \frac{1}{(4n^2 - 1)(2\langle e - n^2\rangle + 1)}, \tag{21}$$

(where if $\langle e/2\rangle = \langle e\rangle$ the sum should be understood to be empty). Thus the derivative $\mathscr{T}'(\alpha)$ is piecewise constant on the critical intervals $\mathscr{I}^e$.

Proof. We differentiate the expression (16) of proposition 1 with respect to α. The function $P^{-1}(x)$ of (17) is differentiable at every x which is not a perfect square, with

$$\frac{dP^{-1}(x)}{dx} = \frac{1}{2\langle x\rangle + 1} \qquad \sqrt{x} \notin \mathbb{Z}.$$

Letting $x = \alpha - n^2$, we have that the derivative exists whenever α cannot be expressed as a sum of squares:

$$\frac{dP^{-1}(\alpha - n^2)}{dx} = \frac{1}{2\langle \alpha - n^2 \rangle + 1} \qquad \alpha \notin \mathscr{E}.$$

Furthermore, the floor in the denominator of the above is constant between two consecutive sums of squares:

$$\langle \alpha - n^2 \rangle = \langle e - n^2 \rangle \qquad \alpha \in \mathscr{I}^e,$$

so that the derivative is constant on each of the critical intervals $\mathscr{I}^e$. Similarly the bounds of the sum in (16) are a function of e only:

$$\langle \alpha/2 \rangle = \langle e/2 \rangle \qquad \langle \alpha \rangle = \langle e \rangle \qquad \alpha \in \mathscr{I}^e.$$

Thus if $\alpha \in \mathscr{I}^e$ is non-critical, then $\mathscr{T}(\alpha)$ is differentiable and

$$\frac{\mathscr{T}'(\alpha)}{4} = \frac{1}{(2\langle e/2 \rangle + 1)^2} - 4 \sum_{n=\langle e/2 \rangle + 1}^{\langle e \rangle} \frac{1}{(4n^2 - 1)(2\langle e - n^2 \rangle + 1)},$$

as required. □

Note that the derivative $\mathscr{T}'(\alpha)$ is not defined at the critical numbers. In what follows, we write $\mathscr{T}'(e)$ to denote the value of $\mathscr{T}'(\alpha)$ on $\mathscr{I}^e$.

3. The integrable asymptotics

In this section we define a time-advance map $\mathscr{F}_\lambda$ of the flow of the hamiltonian $\mathscr{H}$. Here λ is a scaling parameter which controls the speed of the flow; it will be used to match the integrable orbits with those of the rescaled discretised rotation F_λ (3). The map $\mathscr{F}_\lambda$ has a natural recurrence time, and we consider its first return to a Poincaré section aligned along the symmetry line $x = y$. We find that, under a suitable change of coordinates, the first return map within each polygon class is a linear twist map on a cylinder.

Then we consider the behaviour of the Hamiltonian system at infinity, where the index $e \in \mathscr{E}$ diverges. In this limit the number of discontinuities experienced by an orbit (i.e., the number of vertices of the polygons) is unbounded, whilst the magnitude of these discontinuities becomes arbitrarily small. We find that the limiting behaviour is a dichotomy. Typically the limiting flow is linear, like the underlying rigid rotation: however, for a certain subsequence of values of e the nonlinearity persists.

3.1. **The unperturbed return map.** Let $\mathscr{F}_\lambda$ be the following map:

$$\mathscr{F}_\lambda : \mathbb{R}^2 \to \mathbb{R}^2 \qquad \mathscr{F}_\lambda(z) = \varphi_{(\lambda - \mathscr{T}(z))/4}(z), \tag{22}$$

where φ_t is the time-t advance map of the flow, and where we have overloaded the notation $\mathscr{T}$ by writing $\mathscr{T}(z)$ to denote the period of the point $z \in \mathbb{R}^2$. For small λ, the fourth iterates of $\mathscr{F}_\lambda$ produce a small increment of the flow:

$$\mathscr{F}_\lambda^4(z) = \varphi_{\lambda - \mathscr{T}(z)}(z) = \varphi_\lambda(z)$$

where points of the form $\varphi_{\pm\lambda/2}(x, x)$ are identified since they are connected by the action of φ_λ.

We define a first-return map for $\mathscr{F}_\lambda$. For the Poincaré section $\mathscr{X}$ we choose the set of points in the first quadrant which are closer to $\operatorname{Fix} G$ than their preimages under φ_λ, and at least as close as their images:

$$\mathscr{X} = \{\varphi_{\lambda\theta}(x, x) \,:\, x \geqslant 0,\ \theta \in [-1/2, 1/2)\}. \tag{23}$$

Since the period function $\mathscr{T}(\alpha)$ of the flow is piecewise-affine on the critical intervals $\mathscr{I}^e$, we expect the first return map of $\mathscr{F}_\lambda$ to be affine on each of the polygon classes. We isolate the behaviour corresponding to each polygon class by defining a sequence of sub-domains $\mathscr{X}^e \subset \mathscr{X}$, for $e \in \mathscr{E}$, whose union has full measure in $\mathscr{X}$ as $\lambda \to 0$.

The polygon class associated with the critical number $e \in \mathscr{E}$ meets the positive half symmetry line in the box $B_{m,m}$, where $m = \langle e/2 \rangle$, so that the local component of the vector field $\mathbf{w}$ is $\mathbf{w}_{m,m}$. We call a point $z \in \mathscr{X}$ with $\mathscr{H}(z) \in \mathscr{I}^e$ **regular** with respect to the flow if

$$\varphi_\lambda(z) = z + \lambda \mathbf{w}(z) = z + \lambda \mathbf{w}_{m,m}. \tag{24}$$

Then the family of sets $\mathscr{X}^e$ are given by:

$$\mathscr{X}^e = \{z \in \mathscr{X} \,:\, \mathscr{H}(z) \in I^e(\lambda)\} \qquad e \in \mathscr{E}, \tag{25}$$

where $I^e(\lambda) \subset \mathscr{I}^e$ is the largest interval such that all points in $\mathscr{X}^e$ are regular. Since all points which are not regular must lie in an $O(\lambda)$ neighbourhood of the boundary of $B_{m,m}$, it is straightforward to show that $|I^e(\lambda)| \to |\mathscr{I}^e|$ as $\lambda \to 0$.

3.2. **A change of coordinates.** We introduce canonical coordinates for the return map on each polygonal class, which will facilitate the comparison between classes. We let $\mathbb{X}$ denote the unit cylinder:

$$\mathbb{X} = \mathbb{S}^1 \times \mathbb{R}. \tag{26}$$

Then, for $e \in \mathscr{E}$, we define the two-parameter family of maps:

$$\eta_\lambda^e : \mathscr{X}^e \to \mathbb{X} \qquad e \in \mathscr{E},\ \lambda > 0.$$

(We shall often omit the λ-dependence in the notation.) The map η^e_λ is a change of coordinates $z = (x, y) \mapsto (\theta, \rho)$, with

$$\theta(z) = \frac{1}{\lambda}\frac{x-y}{2(2\langle e/2\rangle + 1)} \qquad \rho(z) = \frac{1}{\lambda}\frac{x+y-2x_0}{2(2\langle e/2\rangle + 1)}, \tag{27}$$

where $z_0 = (x_0, x_0) \in \mathscr{X}^e$ is some fixed point of the return map lying on $\operatorname{Fix} G$. (Below, in the proof of theorem 3, we show that such a fixed point is guaranteed to exist for all sufficiently small λ.) This change of coordinates is the composition of several transformations: a rotation through an angle $\pi/4$, which maps the symmetry line $\operatorname{Fix} G$ onto the ρ-axis; a rescaling of the plane by a factor of $1/\lambda\sqrt{2}(2\langle e/2\rangle + 1)$, which normalises the range of the coordinate θ; a translation, which sets the preimage of the origin $(\theta, \rho) = (0, 0)$ at the fixed point z_0.

For $z, \varphi_{\lambda t}(z) \in \mathscr{X}^e$, the flow acts as:

$$\varphi_{\lambda t}(z) = z + \lambda t \mathbf{w}(z),$$

where $\mathbf{w}(z)$ is perpendicular to $\operatorname{Fix} G$ (see equation (24)). Thus the coordinate θ is parallel to the direction of flow, and ρ is perpendicular to it:

$$\varphi_{\lambda t}(\theta, \rho) = (\theta + t, \rho).$$

(We use the symbol φ to denote the flow in both coordinate spaces.) If we identify the interval $[-1/2, 1/2)$ with the unit circle $\mathbb{S}^1$, then we see that the coordinate θ plays the same role as in the expression (23) for $\mathscr{X}$.

In the following proposition, we show that under this change of coordinates, the unperturbed return map becomes a linear twist map.

Theorem 3. *For $e \in \mathscr{E}$, let T^e be the map*

$$T^e : \mathbb{X} \to \mathbb{X} \qquad T^e(\theta, \rho) = (\theta - \kappa\rho,\, \rho)\,. \tag{28}$$

where $\mathbb{X}$ was defined in (26),

$$\kappa(e) = -\frac{1}{2}(2\langle e/2\rangle + 1)^2 \mathscr{T}'(e), \tag{29}$$

and $\mathscr{T}$ is the period function given by (16). Then for any sufficiently small $\lambda > 0$, the following diagram commutes:

$$\begin{array}{ccc} \mathscr{X}^e & \xrightarrow{\mathscr{F}^t_\lambda} & \mathscr{X}^e \\ \downarrow \eta & & \downarrow \eta \\ \mathbb{X} & \xrightarrow{T^e} & \mathbb{X} \end{array}$$

where t is the first-return time to $\mathscr{X}^e$.

Proof. For $e \in \mathscr{E}$, pick $z \in \mathscr{X}^e$ and let $(\theta, \rho) = \eta^e(z)$. Furthermore, suppose that t is the return time of z to $\mathscr{X}^e$, and let $z' = \mathscr{F}^t_\lambda(z)$. We begin by finding an expression for the return time t.

If $z = \varphi_{\lambda\theta}(x, x)$ for some $x \geqslant 0$, then by the definition (22) of $\mathscr{F}_\lambda$ we have

$$\mathscr{F}^k_\lambda(z) = \varphi_{\lambda\theta + k(\lambda - \mathscr{T}(z))/4}(x, x) \qquad k \in \mathbb{Z}.$$

Thus, by the expression (23) for $\mathscr{X}$, the kth iterate of z under $\mathscr{F}_\lambda$ lies in the set $\mathscr{X}$ if and only if

$$\theta + k\left(\frac{\lambda - \mathscr{T}(z)}{4\lambda}\right) + \frac{m\mathscr{T}(z)}{\lambda} \in [-1/2, 1/2)$$

for some $m \in \mathbb{Z}$. The return time t is the minimal $k \in \mathbb{N}$ for which this inclusion holds. Writing $k = 4l + r$ for $l \in \mathbb{Z}_{\geqslant 0}$ and $0 \leqslant r \leqslant 3$, it is straightforward to see that k is minimal when $r = 1$, $m = l$, and l satisfies

$$\theta + l - \frac{\mathscr{T}(z)}{4\lambda} \in [-3/4, 1/4),$$

i.e., when

$$l + \left\lfloor \theta + \frac{3}{4} - \frac{\mathscr{T}(z)}{4\lambda} \right\rfloor = 0.$$

Thus the return time is given by

$$t = 4 \left\lceil \frac{\mathscr{T}(z)}{4\lambda} - \theta - \frac{3}{4} \right\rceil + 1, \tag{30}$$

where we have used the relation $-\lfloor x \rfloor = \lceil -x \rceil$.

Now if $z' = \varphi_{\lambda\theta'}(x, x)$, where $\theta' \in [-1/2, 1/2)$, then by construction, we have

$$\lambda\theta' \equiv \lambda\theta + t\left(\frac{\lambda - \mathscr{T}(z)}{4}\right) \pmod{\mathscr{T}(z)},$$

where we write $a \equiv b \pmod{c}$ for real c to denote that $(a - b) \in c\,\mathbb{Z}$. Thus it follows from the formula (30) for the return time that

$$\begin{aligned}
\lambda\theta' &\equiv \lambda\theta + \lambda\left\lceil \frac{\mathscr{T}(z)}{4\lambda} - \frac{3}{4} - \theta \right\rceil + \frac{\lambda - \mathscr{T}(z)}{4} \pmod{\mathscr{T}(z)} \\
&\equiv -\lambda\left\lfloor \theta + \frac{3}{4} - \frac{\mathscr{T}(z)}{4\lambda} \right\rfloor + \lambda\left(\theta + \frac{3}{4} - \frac{\mathscr{T}(z)}{4\lambda}\right) - \frac{\lambda}{2} \pmod{\mathscr{T}(z)} \\
&\equiv \lambda\left\{\theta + \frac{3}{4} - \frac{\mathscr{T}(z)}{4\lambda}\right\} - \frac{\lambda}{2} \pmod{\mathscr{T}(z)}, \qquad (31)
\end{aligned}$$

where $\{x\}$ denotes the fractional part of x. Since the expression on the right hand side of (31) lies in the interval $[-\lambda/2, \lambda/2)$, equation (31) must in fact be an equality. Thus, dividing through by λ, we obtain

$$\theta' \equiv \theta + \frac{1}{4} - \frac{\mathscr{T}(z)}{4\lambda} \pmod{1}.$$

We wish to apply the change of coordinates η^e. The fixed point z_0 used in the definition of η^e may be any $z \in \mathscr{X}^e$ satisfying $\theta = \theta' = 0$, i.e., $z_0 \in \operatorname{Fix} G$ and

$$0 \equiv \frac{1}{4} - \frac{\mathscr{T}(z_0)}{4\lambda} \pmod{1}. \tag{32}$$

Provided that $\mathscr{T}'(e)$ is non-zero, we can always choose such a z_0 as long as λ is sufficiently small. Then, in the new coordinates, we have

$$\eta^e(z') = \left(\theta + \frac{1}{4} - \frac{\mathscr{T}(z)}{4\lambda}, \rho\right),$$

where we have used the fact that the coordinate θ is periodic.

Now let $z = (x, y)$ and $z_0 = (x_0, x_0)$. Since the Hamiltonian function $\mathscr{H}$ is affine on $\mathscr{X}^e$, expanding $\mathscr{H}$ about z_0 gives

$$\begin{aligned}
\mathscr{H}(z) &= \mathscr{H}(z_0) + (x + y - 2x_0)(2\langle e/2\rangle + 1) \\
&= \mathscr{H}(z_0) + 2\lambda(2\langle e/2\rangle + 1)^2\rho. \qquad (33)
\end{aligned}$$

Similarly, since $\mathscr{T}$ is affine on the interval $\mathscr{I}^e$:

$$\mathscr{T}(z) = \mathscr{T}(z_0) + 2\lambda(2\langle e/2\rangle + 1)^2\rho\mathscr{T}'(e).$$

Finally, using the property (32) of the fixed point z_0, we have

$$\begin{aligned}
\eta^e(z') &= \left(\theta + \frac{1}{4} - \frac{\mathscr{T}(z_0) + 2\lambda(2\langle e/2\rangle + 1)^2\rho\mathscr{T}'(e)}{4\lambda}, \rho\right) \\
&= \left(\theta - \frac{1}{2}(2\langle e/2\rangle + 1)^2\rho\mathscr{T}'(e), \rho\right),
\end{aligned}$$

which completes the proof. □

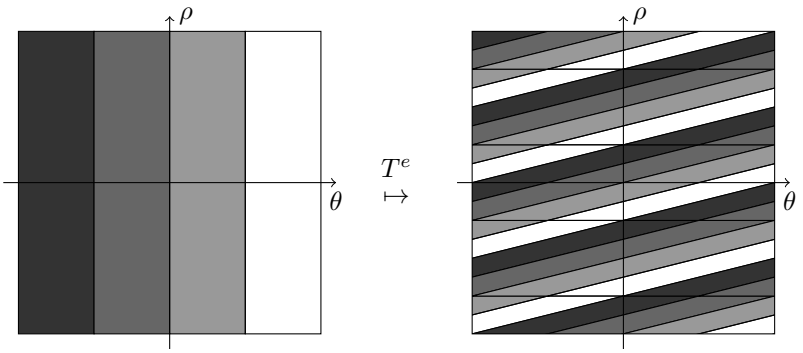

FIGURE 6. A schematic representation of the action of the twist map T^e on the space $\mathbb{X} = \mathbb{S}^1 \times \mathbb{R}$

Note that the action of the conjugate map T^e is independent of the parameter λ, which appears only in the domain $\eta^e_\lambda(\mathscr{X}^e)$ in which the conjugate map is valid. Using the definition (25) of the domain $\mathscr{X}^e$ and the above expansion (33) of $\mathscr{H}$ about the fixed point z_0, we see that this domain is given by

$$\eta^e_\lambda(\mathscr{X}^e) = \{(\theta,\rho) \in \mathbb{X} : \mathscr{H}(z_0) + 2\lambda(2\langle e/2\rangle + 1)^2\rho \in I^e(\lambda)\}.$$

The range of values of ρ in the domain grows like

$$\frac{|I^e(\lambda)|}{2\lambda(2\langle e/2\rangle + 1)^2} = \frac{|\mathscr{I}^e|}{2\lambda(2\langle e/2\rangle + 1)^2} + O(1)$$

as $\lambda \to 0$, and in the integrable limit, we think of the conjugate map as valid on the whole of $\mathbb{X}$.

For $e \in \mathscr{E}$, let us consider the twist $\kappa(e)$ of the map T^e, given in (29). Each T^e is reversible, and can be written as the composition of the involutions G and H^e, where

$$G(\theta,\rho) = (-\theta,\rho) \qquad H^e(\theta,\rho) = (-\theta + \rho\kappa(e),\ \rho)\,.$$

We use the same symbol G to denote the reversing symmetry on the plane (equation (13)) and on the cylinder. The fixed spaces of these involutions are given by

$$\operatorname{Fix} G = \{(\theta,\rho) \in \mathbb{X} : \theta \in \{-1/2, 0\}\},$$
$$\operatorname{Fix} H^e = \{(\theta,\rho) \in \mathbb{X} : \theta = -\frac{1}{2}\rho\kappa(e)\}. \tag{34}$$

The map T^e is also reversible with respect to the reflection $(\theta,\rho) \mapsto (\theta,-\rho)$, and equivariant under the group generated by the translation

$$\rho \mapsto \rho + \rho^* \qquad \rho^* = \frac{1}{\kappa(e)} = \frac{-2}{(2\langle e/2\rangle + 1)^2\mathscr{T}'(e)}. \tag{35}$$

Each circle $\rho = $ const. is invariant under T^e, and motion restricted to this circle is a rotation with rotation number ρ/ρ^* (mod 1).

3.3. **The integrable return map at infinity.** Now we are in a position to study the dynamics of the sequence of maps T^e in the limit $e \to \infty$. As in section 2.1, where we studied the nonlinearity of the flow, we turn our attention to the behaviour of the period function $\mathscr{T}$.

As $\alpha \to \infty$, the period $\mathscr{T}(\alpha)$ converges to π, which is the period of the rotation with Hamiltonian $\mathscr{Q}(x,y) = x^2 + y^2$. Furthermore, the period undergoes damped oscillations about its limiting value [RB14]. If we write

$$\alpha(n,b) = (n+b)^2 \qquad n \in \mathbb{N},\ b \in [0,1), \tag{36}$$

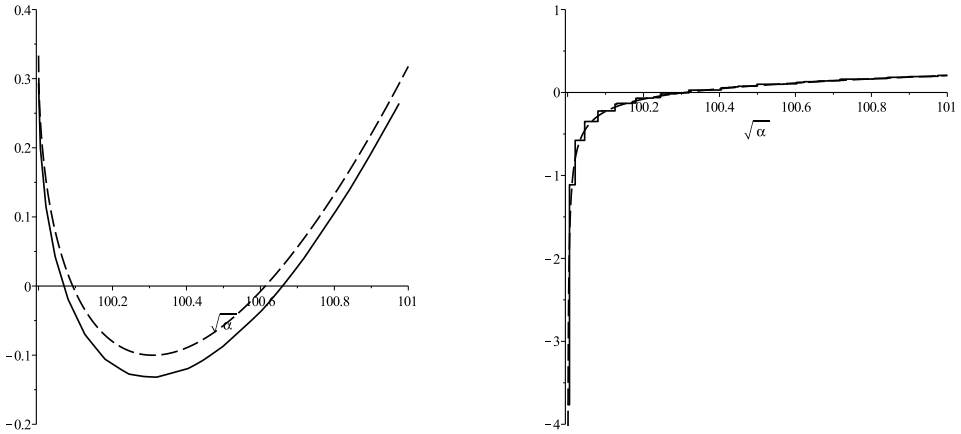

FIGURE 7. Left: the function $\langle\alpha\rangle^{3/2}\left(\mathscr{T}(\alpha)-\pi\right)/4$ (solid line) against $\sqrt{\alpha}$ for $\sqrt{\alpha}\in[100,101)$, i.e., for $n=\langle\alpha\rangle=100$ and $b=\{\sqrt{\alpha}\}\in[0,1)$. The dotted line shows the function $\frac{1}{3}(2b+1)^{3/2}-\sqrt{2b}$. Right: the function $\frac{1}{2}(2\langle\alpha/2\rangle+1)^2\mathscr{T}'(\alpha)$ of equation (35) (solid line). The dotted lines show the approximate limiting function (57).

so that n is the integer part of $\sqrt{\alpha(n,b)}$ and b is the fractional part, then one can show that the following limiting function exists:

$$\lim_{n\to\infty}\left(n^{3/2}(\mathscr{T}(\alpha(n,b))-\pi)\right),$$

and is described qualitatively by the following function of the unit interval

$$b\mapsto\frac{1}{3}(2b+1)^{3/2}-\sqrt{2b} \tag{37}$$

(see figure 7). The key feature of this limiting function is the singularity in its derivative at $b=0$.

With $\alpha(n,b)$ as in (36), we let $e(n,b)$ be the critical number associated with α:

$$(n+b)^2\in\{e(n,b)\}\cup\mathscr{I}^{e(n,b)}\qquad\qquad n\in\mathbb{N},\ b\in[0,1). \tag{38}$$

Then the behaviour of the sequence of twists $\kappa(e(n,b))$ as $n\to\infty$ is described by the following theorem.

Theorem 4. *Let $b\in[0,1)$ and let $e(n,b)$ be given as in* (38)*. Then as $n\to\infty$:*

$$\kappa(e(n,b))\to\begin{cases}4 & x=0,\\ 0 & \text{otherwise.}\end{cases}. \tag{39}$$

Proof. Take $\alpha\geqslant 0$ and let $e\in\mathscr{E}$ be such that $\alpha\in\mathscr{I}^e$. From the formula (21) for the derivative of the period function, we have

$$\frac{1}{2}(2\langle e/2\rangle+1)^2\mathscr{T}'(\alpha)=2-8(2\langle e/2\rangle+1)^2\sum_{k=\langle e/2\rangle+1}^{\langle e\rangle}\frac{1}{(4k^2-1)(2\langle\alpha-k^2\rangle+1)}. \tag{40}$$

(Recall that if $\alpha\in\mathscr{I}^e$ for some $e\in\mathscr{E}$, the expression in the denominator of the summand satisfies $\langle\alpha-k^2\rangle=\langle e-k^2\rangle$.)

We consider the summand in (40). For k in the range $\langle e/2\rangle+1\leqslant k\leqslant\langle e\rangle-1$, we have

$$\frac{1}{(4k^2-1)(2\lfloor\sqrt{\alpha-k^2}\rfloor+1)}=\frac{1}{8k^2\sqrt{\alpha-k^2}}\left(1-\frac{1}{4k^2}\right)^{-1}\left(1-\frac{\{\sqrt{\alpha-k^2}\}-1/2}{\sqrt{\alpha-k^2}}\right)^{-1}.$$

Here the square root is bounded below by

$$\sqrt{\alpha - k^2} \geqslant \sqrt{\langle e\rangle^2 - (\langle e\rangle - 1)^2} = \sqrt{2\langle e\rangle - 1} > \alpha^{1/4},$$

whereas $k^2 > \alpha/2$. Hence as $\alpha \to \infty$, we have

$$\frac{1}{(4k^2-1)(2\lfloor\sqrt{\alpha-k^2}\rfloor+1)} = \frac{1}{8k^2\sqrt{\alpha-k^2}}\left(1+O\left(\frac{1}{\alpha^{1/4}}\right)\right). \tag{41}$$

Summing over k, we can approximate all but the $k = \langle e\rangle$ term sum with an integral:

$$\begin{aligned}\sum_{k=\langle e/2\rangle+1}^{\langle e\rangle-1} \frac{1}{k^2\sqrt{\alpha-k^2}} &= \int_{\langle e/2\rangle+1/2}^{\langle e\rangle-1/2} \frac{1}{x^2\sqrt{\alpha-x^2}}\left(1+O\left(\frac{1}{\alpha^{1/4}}\right)\right)dx \\ &= \frac{1}{\alpha}\Big[\tan\theta\Big]_{\theta_2}^{\theta_1}\left(1+O\left(\frac{1}{\alpha^{1/4}}\right)\right)\end{aligned}$$

where we have used the substitution $x = \sqrt{\alpha}\cos\theta$, and the limits θ_1 and θ_2 satisfy:

$$\cos\theta_1 = \frac{\langle e/2\rangle + 1/2}{\sqrt{\alpha}} \qquad \cos\theta_2 = \frac{\langle e\rangle - 1/2}{\sqrt{\alpha}}.$$

Using Taylor's Theorem, we find that $\tan\theta_1$ and $\tan\theta_2$ are given by

$$\tan\theta_1 = 1 + O\left(\frac{1}{\sqrt{\alpha}}\right) \qquad \tan\theta_2 = O\left(\frac{1}{\alpha^{1/4}}\right),$$

so that

$$\sum_{k=\langle e/2\rangle+1}^{\langle e\rangle-1} \frac{1}{k^2\sqrt{\alpha-k^2}} = \frac{1}{\alpha}\left(1+O\left(\frac{1}{\alpha^{1/4}}\right)\right). \tag{42}$$

Applying (41) and (42) to the sum in (40), we obtain

$$\begin{aligned}&8(2\langle e/2\rangle+1)^2 \sum_{k=\langle e/2\rangle+1}^{\langle e\rangle-1} \frac{1}{(4k^2-1)(2\langle\alpha-k^2\rangle+1)} \\ &= (2\langle e/2\rangle+1)^2 \sum_{k=\langle e/2\rangle+1}^{\langle e\rangle-1} \frac{1}{k^2\sqrt{\alpha-k^2}}\left(1+O\left(\frac{1}{\alpha^{1/4}}\right)\right) \\ &= \frac{1}{\alpha}(2\langle e/2\rangle+1)^2\left(1+O\left(\frac{1}{\alpha^{1/4}}\right)\right) \\ &= 2 + O\left(\frac{1}{\alpha^{1/4}}\right)\end{aligned}$$

as $\alpha \to \infty$. Thus substituting this back into (40), we see that only the $k = \langle e\rangle$ term remains. If $\alpha = (n+b)^2$, then $\langle e\rangle = n$, and the remaining term is given by:

$$\begin{aligned}\frac{1}{2}(2\langle e/2\rangle+1)^2\mathscr{T}'(\alpha) &= \frac{-8(2\langle e/2\rangle+1)^2}{(4n^2-1)\,(2\langle\alpha-n^2\rangle+1)} + O\left(\frac{1}{\alpha^{1/4}}\right) \\ &= \frac{-4}{2\langle 2nb+b^2\rangle+1}\left(1+O\left(\frac{1}{\sqrt{\alpha}}\right)\right) + O\left(\frac{1}{\alpha^{1/4}}\right). \qquad (43)\end{aligned}$$

If $b > 0$, then

$$\frac{1}{2\langle 2nb+b^2\rangle+1} \to 0$$

as $n \to \infty$. Thus the remaining term in (43) goes to zero and $(2\langle e/2\rangle+1)^2\mathscr{T}'(\alpha)$ vanishes in the limit. However, if $b = 0$, then we have

$$\frac{1}{2}(2\langle e/2\rangle+1)^2\mathscr{T}'(\alpha) = -4 + O\left(\frac{1}{\alpha^{1/4}}\right).$$

□

The convergence (39) is not uniform: if b is close to zero, the convergence can be made arbitrarily slow. For a plot of $(2\langle e/2\rangle + 1)^2 \mathscr{T}'(\alpha)/2$, see figure 7.

The two regimes of behaviour for the sequence of return maps T^e follow directly.

Corollary 5. *Let $b \in [0, 1)$ and let $e(n, b)$ be given as in (38). If $b = 0$, then the sequence $e(n, b)$ is simply the sequence of perfect squares, and as $n \to \infty$, the sequence of functions $T^{e(n,b)}$ converges pointwise to a limiting function T^∞ given by*

$$T^\infty : \mathbb{X} \to \mathbb{X} \qquad T^\infty(\theta, \rho) = (\theta + 4\rho, \rho)\,.$$

If $b > 0$, then the sequence $T^{e(n,b)}$ converges pointwise to the identity.

The (reversing) symmetries of $T^{e(n,b)}$ also converge as $n \to \infty$, leading to an asymptotic version of H^e. Here we note in particular the translation invariance (35) of the sequence $T^{e(n,b)}$, whose magnitude satisfies

$$|\rho^*| \to \begin{cases} 1/4 & b = 0 \\ \infty & b > 0 \end{cases} \tag{44}$$

as $n \to \infty$.

4. The perturbed dynamics

Let us return to the perturbed dynamics, i.e., to the rescaled discretised rotation F_λ. We saw that under a suitable change of coordinates, the unperturbed return map corresponds to a linear twist map T^e on the cylinder, whose dependence on the parameter is singular in the limit $e \to \infty$. There is a corresponding perturbed twist map Φ of a discretised cylinder, which captures the recurrent behaviour of F_λ. As $e \to \infty$ through a sub-sequence of (e_i) (cf. (8)), we get a sequence of discrete twist maps with vanishing discretisation length. The resulting dynamics will depend on the particular sub-sequence chosen. In the regime where the twist vanishes in the limit, the round-off fluctuations result in intricate resonance structures, reminiscent of the island chains of near-integrable Hamiltonian systems. Conversely, in the regime where the twist persists, there are no discernible phase space features and a form of 'pseudochaos' emerges.

Throughout what follows, we adopt an informal approach, focussing on qualitative observations and numerical evidence.

4.1. **The perturbation mechanism.** The correspondence between the integrable flow described in the previous sections and the behaviour of the rescaled lattice map F_λ in the limit $\lambda \to 0$ is illustrated by the following proposition, which is a simple consequence of [RBV13, Proposition 1]. It says that, within a bounded region of the plane, the lattice points over which the time-advance map and the round-off dynamics agree have full density as $\lambda \to 0$.

Proposition 6. *For $r > 0$, we define the set*

$$A(r,\lambda) = \{z \in (\lambda\mathbb{Z})^2 \,:\, \|z\|_\infty < r\} \tag{45}$$

(with $\|(u,v)\|_\infty = \max(|u|,|v|)$). Then

$$\lim_{\lambda\to 0} \frac{\#\{z \in A(r,\lambda) \,:\, \varphi_\lambda(z) = F_\lambda^4(z)\}}{\#A(r,\lambda)} = 1.$$

We isolate the lattice points $z \in (\lambda\mathbb{Z})^2$ where the fourth iterates of F_λ deviate from the time-advance map φ_λ by defining the set Λ of **transition points**. We say that a point $z \in (\lambda\mathbb{Z})^2$ is a transition point if z and its image under F_λ^4 do not belong to the same box. Then

$$\Lambda = \bigcup_{m,n\in\mathbb{Z}} \Lambda_{m,n}, \tag{46}$$

where

$$\Lambda_{m,n} = F_\lambda^{-4}(B_{m,n} \cap (\lambda\mathbb{Z})^2) \setminus B_{m,n}.$$

For sufficiently small λ, all points $z \neq (0,0)$ where $F_\lambda^4(z) \neq z + \lambda\mathbf{w}(z)$ are transition points [RBV13, Lemma 4]. Hence F_λ^4 is equal to the time-λ advance of the flow everywhere except at the transition points.

Proposition 7. *Let $A(r,\lambda)$ be as in equation (45). Then for all $r > 0$ there exists $\lambda^* > 0$ such that, for all $\lambda < \lambda^*$ and $z \in A(r,\lambda)$, we have*

$$z \notin \Lambda \cup \{(0,0)\} \quad \Rightarrow \quad F_\lambda^4(z) = \varphi_\lambda(z).$$

The transition points play the role of the vertices for the perturbed orbits, and are the basis of the strip-map construction for the map F_λ: for small λ, the set of transition points consists of thin strips of lattice points arranged along the lines Δ (see figure 8). The **strip map** Ψ is the transit map to Λ, which is defined as follows:

$$\Psi : (\lambda\mathbb{Z})^2 \to \Lambda \qquad \Psi(z) = F_\lambda^{4t(z)}(z), \tag{47}$$

where the transit time t to Λ is well-defined for all points excluding the origin. (Since the origin plays no role in the present construction, to simplify notation we shall write $(\lambda\mathbb{Z})^2$ for $(\lambda\mathbb{Z})^2 \setminus$

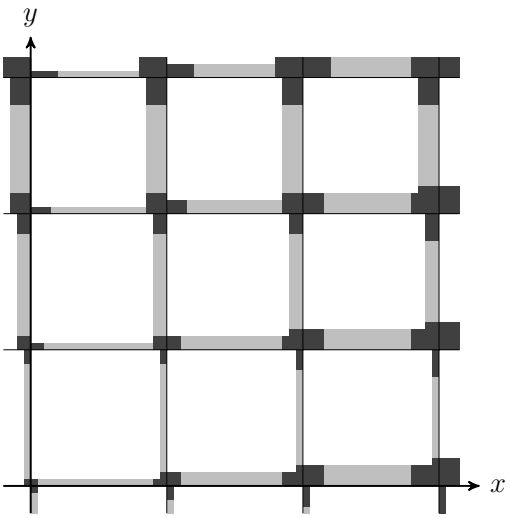

FIGURE 8. Structure of phase space. The boxes $B_{m,n}$, bounded by the set Δ, include regular domains (white), where the motion is integrable. The light grey regions comprise the set Λ of transition points, given in (46). The dark grey regions near the integer lattice $\mathbb{Z}^2$ is the set Σ. The orbits that intersect it are the perturbed analogue of the critical polygons, and are excluded from our analysis.

$\{(0,0)\}$, where appropriate.) The strip map moves points parallel to the relevant component of the piecewise-constant vector field $\mathbf{w}$, with a possible additional small perturbation. If $z \in \Lambda_{m,n}$:

$$\Psi(z) = z + \lambda t(z)\mathbf{w}_{m,n} + \lambda(\mathbf{v}(z) - \mathbf{w}(z)). \tag{48}$$

We shall exclude the regions of the phase space where multiple strips overlap, which form a set $\Sigma \subset (\lambda\mathbb{Z})^2$, clustered around the lattice points of $\mathbb{Z}^2$ [RBV13, Section 5]. Thus we exclude the orbits that intersect this set —the so called **critical orbits**.

In [RBV13, section 3], we defined a Poincaré return map Φ on a neighbourhood X of the positive half of the symmetry line $\operatorname{Fix} G$. For time-scales corresponding to a first return to the domain X, every integrable orbit has a scaled return orbit that shadows it [RBV13, theorem 5]. The orbits which are not critical form a sequence of subsets X^e of X, $e \in \mathscr{E}$, which correspond to the polygon classes of the flow. The set X^e is the intersection of the lattice $(\lambda\mathbb{Z})^2$ with a thin rectangle lying along the symmetry line $\operatorname{Fix} G$:

$$X^e = \{\lambda(x,y) \in (\lambda\mathbb{Z})^2 \,:\, -(2\langle e/2\rangle + 1) \leqslant x - y < 2\langle e/2\rangle + 1,\ \mathscr{P}(\lambda x, \lambda y) \in I^e(\lambda)\}, \tag{49}$$

where, just as in equation (25), the set $I^e(\lambda)$ is a subset of $\mathscr{I}^e$ whose length tends to that of $\mathscr{I}^e$ as $\lambda \to 0$ [RBV13, Proposition 6]:

$$\lim_{\lambda\to 0} \frac{|I^e(\lambda)|}{|\mathscr{I}^e|} = 1.$$

From this it follows that the sets X^e have full density in X as $\lambda \to 0$. We identify opposite sides of the set X^e which are connected by the local vector field so that the dynamics takes place on a lattice on a cylinder.

For orbits which are not critical, the return map Φ can be constructed from repeated iterations of the strip map. For $e \in \mathscr{E}$ and $z \in X^e$:

$$\Phi(z) \equiv (\Psi^{2\langle e\rangle+2} \circ F_\lambda)(z) \pmod{\lambda\mathbf{w}(z)}, \tag{50}$$

where the modulus reflects the periodicity of the transversal coordinate. (Here we write $(\mathrm{mod}\ \mathbf{a})$ for some vector $\mathbf{a}$ to denote congruence modulo the one-dimensional module generated by $\mathbf{a}$.)

Relative to the integrable flow, each iterate of the strip map Ψ produces an elementary perturbation of the type described in the introduction (figure 1), and the number of such perturbations which contribute to the return map Φ diverges as $e \to \infty$.

4.2. **The perturbed return map.** We turn our attention to the reversing symmetry group of the return map Φ, which is inherited from the reversing symmetry G of the lattice map F_λ (see equation (13)). In the following proposition we describe the form of this reversing symmetry on the domains X^e (equation (49)). Then we apply the change of coordinates η^e from the previous section to the domain X^e and compare the properties of the resulting discrete perturbed twist map to that of the unperturbed twist map T^e.

Proposition 8. *For $e \in \mathscr{E}$, let G^e be the involution of X^e given by*

$$G^e(x,y) = \begin{cases} (y,x) & |x-y| < \lambda(2\langle e/2\rangle + 1) \\ (x,y) & x - y = -\lambda(2\langle e/2\rangle + 1). \end{cases} \tag{51}$$

Then for all sufficiently small λ, G^e is a reversing symmetry of Φ on X^e in the following sense:

$$\forall z, \Phi(z) \in X^e : \qquad \Phi^{-1}(z) = (G^e \circ \Phi \circ G^e)(z).$$

Proof. Recall that $X^e \subset B_{m,m} \setminus \Lambda$, where $m = \langle e/2\rangle$, so that if $z \in X^e$, then

$$F_\lambda^4(z) = z + \lambda \mathbf{w}(z) = z + \lambda \mathbf{w}_{m,m}.$$

Furthermore, if z lies on the line $x - y = -\lambda(2\langle e/2\rangle + 1)$, then by the definition (12) of the auxiliary vector field, we have

$$G(z) = z + \lambda \mathbf{w}_{m,m}.$$

Combining the above, we have the following relationship between G^e and G:

$$G^e(x,y) = \begin{cases} G(x,y) & |x-y| < \lambda(2\langle e/2\rangle + 1), \\ (F_\lambda^{-4} \circ G)(x,y) & x - y = -\lambda(2\langle e/2\rangle + 1). \end{cases} \tag{52}$$

If $\tau = \tau(z)$ is the return time of z, then by construction

$$\Phi(z) = F_\lambda^\tau(z),$$

and the reversibility of F_λ with respect to G gives us that

$$(G \circ \Phi)(z) = (F_\lambda^{-\tau} \circ G)(z). \tag{53}$$

Suppose now that neither z nor $\Phi(z)$ lies on the line $x - y = -\lambda(2\langle e/2\rangle + 1)$. Then combining (52) and (53) gives

$$(G^e \circ \Phi)(z) = (F_\lambda^{-\tau} \circ G^e)(z).$$

Furthermore, this point lies in X^e, so that

$$(G^e \circ \Phi)(z) = (\Phi^{-1} \circ G^e)(z),$$

as required.

Suppose now that $\Phi(z)$ lies on the line $x - y = -\lambda(2\langle e/2\rangle + 1)$ but z does not. In this case, combining (52) and (53) gives

$$(G^e \circ \Phi)(z) = (F_\lambda^{-4} \circ G \circ \Phi)(z) = (F_\lambda^{-(\tau+4)} \circ G)(z) = (\Phi^{-1} \circ G^e)(z).$$

The other cases proceed similarly. □

Note that the reversing symmetry G^e is simply an adaptation of the original reversing symmetry G of F_λ.

Recall the map T^e (equation (9)), which corresponds to the unperturbed return map under the change of coordinates $\eta^e(\lambda) : (x,y) \mapsto (\theta,\rho)$ of equation (27). In the integrable limit $\lambda \to 0$, the image of the return domain $\mathscr{X}^e$ under η^e approaches the unit cylinder $\mathbb{X}$. The domain

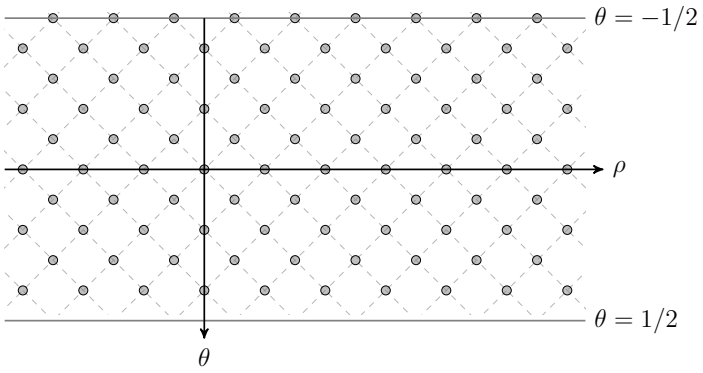

FIGURE 9. The image of the domain X^e under the change of coordinates $\eta^e_\lambda : (\lambda\mathbb{Z})^2 \to \mathbb{X}$. There are $2\langle e/2\rangle + 1$ lattice points per unit length in each of the coordinate directions.

X^e of the perturbed return map Φ is a subset of $\mathscr{X}^e$, thus we can also apply the change of coordinates η^e to X^e. Using the definition (49) of X^e, we see that its image under η^e approaches the following set[1] (see figure 9):

$$\left\{ \frac{1}{2(2\langle e/2\rangle + 1)} (i, i + 2j) \,:\, i, j \in \mathbb{Z},\ -(2\langle e/2\rangle + 1) \leqslant i < 2\langle e/2\rangle + 1 \right\} \subset \mathbb{X}. \tag{54}$$

(The image of the point $\lambda(x, y)$ corresponds to $i = x - y$ and $j = y - x_0$.) This set is a rotated square lattice in the unit cylinder, with lattice spacing $1/\sqrt{2}(2\langle e/2\rangle + 1)$. Thus $e \to \infty$ corresponds to the continuum limit. We think of the dynamics of Φ as taking place in the (θ, ρ) coordinates, and of Φ as a discrete version of T^e.

The map T^e is a linear twist map, with characteristic length scale ρ^* in the ρ-direction (see equation (35)). The map Φ can be considered as a perturbation of T^e which originates from space discretisation. As $e \to \infty$, the fluctuations caused by the perturbation are small relative to the width of the cylinder, do not have any obvious structure, and affect the dynamics in both the ρ and θ directions.

4.3. **Qualitative description and phase plots.** Recall the sequence $e(n, b)$ of critical numbers defined in (38). By corollary 5, if $b \neq 0$, then the sequence of maps $T^{e(n,b)}$ converge non-uniformly to the identity as $n \to \infty$, whereas if $b = 0$, then $T^{e(n,b)}$ converges to the map $(\theta, \rho) \mapsto (\theta + 4\rho, \rho)$. Accordingly, the characteristic length scale ρ^* of the twist dynamics is also singular in the limit, with $|\rho^*| \to \infty$ or $\rho^* \to 1/4$, for the $b \neq 0$ and $b = 0$ cases, respectively (see equation (44)).

We define the **rotation number** ν of a point on the cylinder to be its rotation number under the twist map T^e, i.e.,

$$\nu(\theta, \rho) = \frac{\rho}{\rho^*} \pmod 1 \qquad (\theta, \rho) \in \mathbb{X}.$$

Similarly for a point $z \in X^e$, we write $\nu(z)$ to denote the rotation number of the corresponding point $\eta^e(z)$ on the cylinder. Subsets of the cylinder of the form

$$\{(\theta, \rho) \,:\, \nu(\theta, \rho) - m \in [-1/2, 1/2)\} \subset \mathbb{X} \qquad m \in \mathbb{Z} \tag{55}$$

[1]Recall that in the definition of η^e, the pre-image of the origin is some fixed point z_0 of the unperturbed dynamics. In the discrete case we round z_0 onto the lattice. The choice of the fixed point z_0 will have no bearing on the qualitative or statistical properties of the dynamics.

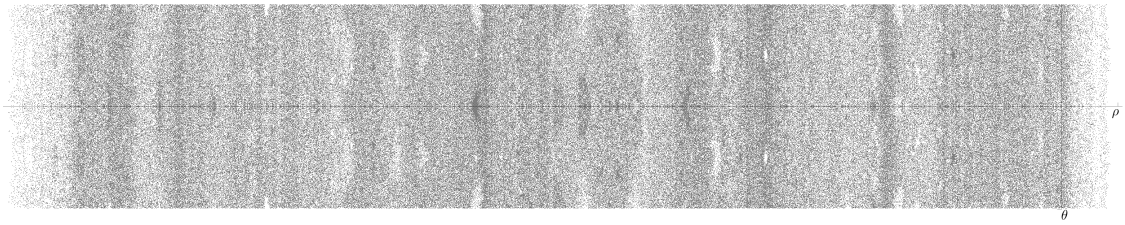

(a) $e = 40000 = 200^2$

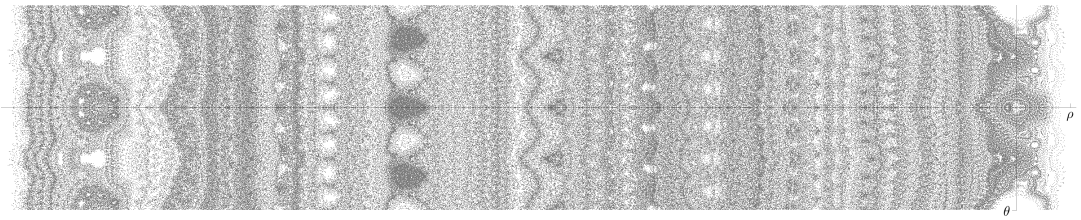

(b) $e = 40309 \approx 200.8^2$

FIGURE 10. Two pixel plots showing a large number of symmetric orbits of the return map Φ in the cylindrical coordinates $(\theta, \rho) \in \mathbb{X}$. The resolution is such that the width of the cylinder (the θ direction) consists of approximately 280 lattice sites. In both cases, the orbits plotted occupy almost half of the region of phase space pictured. The stark contrast between the two plots is caused by the difference in the twist $\kappa(e)$: in plot (a) $\kappa(e) \approx 4$, whereas in plot (b) $\kappa(e) \approx -0.1$. The values of λ used are (a) $\lambda \approx 7 \times 10^{-9}$ and (b) $\lambda \approx 4 \times 10^{-8}$. In figure (b), the primary resonance at the origin is clearly visible, whereas a period 2 resonance, which occurs at $\rho = 1/2K(e)$, is seen to the left of the plot.

are referred to as **fundamental domains** of the dynamics. The number N of lattice points of $\eta^e(X^e)$ per fundamental domain varies like

$$N \sim 2(2\langle e/2\rangle + 1)^2 |\rho^*| \tag{56}$$

as $e \to \infty$. For a given value of e, we expect the dynamics of Φ to be qualitatively the same in each fundamental domain, but to vary locally according to the rotation number. Consequently, in order to observe the global behaviour of Φ, we need to sample whole fundamental domains. However, this is made difficult by the divergence of ρ^* for $b \neq 0$.

To better understand the divergence of ρ^*, we consider the limiting form (37) of the period function $\mathscr{T}(\alpha)$. By differentiating the function (37) (see figure 7) we expect, for large e, the piecewise-constant function $\mathscr{T}'(\alpha)$ to behave approximately as

$$\frac{1}{2}(2\langle \alpha/2\rangle + 1)^2 \mathscr{T}'(\alpha) \approx \frac{2}{\sqrt{n}} \left(\sqrt{2b+1} - 1/\sqrt{2b} \right) \qquad \alpha = (n+b)^2, \quad b \neq 0. \tag{57}$$

By (35), this leads us to expect that

$$\rho^*(\alpha) \approx -\frac{\sqrt{n}}{2} \left(\sqrt{2b+1} - 1/\sqrt{2b} \right)^{-1} \qquad b \neq 0. \tag{58}$$

Figure 11 shows that this rough analysis is valid, although the relationship between the two functions is far from uniform.

Thus we see that $\rho^*(\alpha(n,b))$ typically grows slowly, like $\sqrt{n}$, except near $b = (-1+\sqrt{5})/4 \approx 0.3$, where our approximate form for the derivative $\mathscr{T}'$ is zero. We can exploit this behaviour to examine orbits of Φ in domains X^e where the twist $\kappa(e)$ of T^e is large ($b = 0$ —see figure 10(a)), moderate ($b = 0.8$ —see figure 10(b)) or almost zero ($b = 0.3$ —see figure 4).

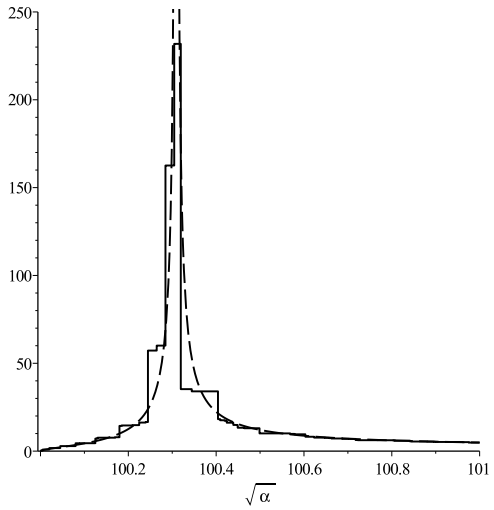

FIGURE 11. A plot of $|\rho^*|$ of equation (35) against $\sqrt{\alpha}$ for $\sqrt{\alpha} \in [100, 101)$, i.e., for $\langle\alpha\rangle = 100$ and $b = \{\sqrt{\alpha}\} \in [0, 1)$ (solid line). The dotted line shows the approximate limiting function (58).

			$\Delta\rho$		$\Delta\nu$	
e	$\langle e\rangle$	ρ^*	Median	Maximum	Median	Maximum
10 000	100	0.266	0.18	0.65	0.69	2.5
40 000	200	0.259	0.16	0.55	0.63	2.1
160 000	400	0.257	0.14	0.48	0.54	1.9
640 000	800	0.255	0.13	0.49	0.51	1.9

(a) $b = 0$

			$\Delta\rho$		$\Delta\nu$	
e	$\langle e\rangle$	ρ^*	Median	Maximum	Median	Maximum
10 057	100	163	0.14	2.9	8.7×10^{-4}	1.8×10^{-2}
40 113	200	106	0.25	2.0	2.3×10^{-3}	1.9×10^{-2}
160 234	400	4105	4.8	8.5	1.2×10^{-3}	2.1×10^{-3}

(b) $b = 0.3$

TABLE 1. A table showing the values of ρ^* for various values of e, and the typical range $\Delta\rho$ and $\Delta\nu$ of $\rho(z)$ and $\nu(z)$, respectively, along orbits. The distribution of the range was calculated according to the fraction of points sampled whose orbit has the given range.

What we see in the case of vanishing twist ($b \neq 0$) is a sea of resonance-like structures, resembling the island chains in a near-integrable Hamiltonian system. The global periodicity of the twist map recedes to infinity, and the phase portrait is determined by the local rotation number. Although orbits may wander over a significant range in the ρ-direction, the variation of the rotation number $\nu(z)$ along orbits is vanishingly small (see table 1(b)).

In the $b = 0$ case the global structure remains, and phase portraits appear featureless. The typical variation in the rotation number along orbits is $1/2$ (see table 1(a)), leading to orbits which typically do not cluster in the θ-direction. In this case it makes sense to consider the statistical properties of orbits of Φ, and in the next section we consider their period distribution function.

4.4. **The period distribution function.** For $e = n^2$, i.e., $b = 0$, we wish to investigate whether the dynamics of Φ are sufficiently disordered that its period statistics are those of random reversible dynamics. The following result provides the relevant probabilistic model:

Theorem 9. [RV09, Theorem A] *Let (G, H) be a pair of random involutions of a set Ω with N points, and let*

$$g = \#\mathrm{Fix}\, G \qquad h = \#\mathrm{Fix}\, H \qquad \gamma = \frac{2N}{g+h}.$$

Let $\mathscr{D}_N(x)$ be the expectation value of the fraction of Ω occupied by periodic orbits of $H \circ G$ with period less than γx, computed with respect to the uniform probability. If, with increasing N, g and h satisfy the conditions

$$\lim_{N\to\infty} g(N) + h(N) = \infty \qquad \lim_{N\to\infty} \frac{g(N)+h(N)}{N} = 0, \tag{59}$$

then for all $x \geqslant 0$, we have the limit

$$\mathscr{D}_N(x) \to \mathcal{R}(x) = 1 - e^{-x}(1+x).$$

Moreover, almost all points in Ω belong to symmetric periodic orbits.

The lattice periodicity of Φ [RBV13, section 5] provides a finite set —a discrete torus— over which to define the period distribution function $\mathscr{D}^e$ of Φ. However, as $e \to \infty$, the size of the space grows super-exponentially, making an exhaustive computation infeasible [RB14]. However, all is not lost: if $e = n^2$ is a square, then the phase portrait is uniform, and it makes sense to sample the space over the much smaller characteristic length ρ^* of the unperturbed twist map T^e. Furthermore, numerical experiments show that the ρ-excursion of a typical periodic orbit is smaller than ρ^*. These circumstances will allow us to estimate the global period distribution function from local data.

We describe an extensive numerical experiment in which we calculate the period distribution function of Φ over suitably chosen invariant sets, along the subsequence of perfect squares $e = n^2$. The results suggests that, as $e \to \infty$, the distribution of periods approaches the distribution $\mathcal{R}(x)$ of theorem 9, and thus is consistent with random reversible dynamics. As in the case of the random reversible map, we observe that symmetric periodic orbits dominate.

$\langle e \rangle$	m	Sample size	$\int(\mathcal{R}-\mathscr{D})dx$	Approx. time
100	32	350 000	0.03	15sec
200	32	1 360 000	0.04	2min
400	32	5 370 000	0.06	15min
800	32	21 200 000	0.06	2hr
1600	16	42 900 000	0.11	11hr

TABLE 2. Some data relating to the calculation of distributions $\mathscr{D}$ for various values of n, and their corresponding maximum values of m. For a given value of m, nine distinct distributions were calculated: for three different values of λ, each with three different values of z_0 (recall $z_0 = (\eta^e)^{-1}(0,0)$). Neither the value of λ nor z_0 was found to have any discernible effect on the distribution. The sample size refers to the number of points sampled during the calculation of each distribution, similarly for the approximate computation time. The integral $\int(\mathcal{R}-\mathscr{D})dx$ was calculated over the interval $[0, 16]$ (every experimental distribution satisfies $\mathscr{D}(16) = 1$), and was averaged over the nine individual distributions calculated.

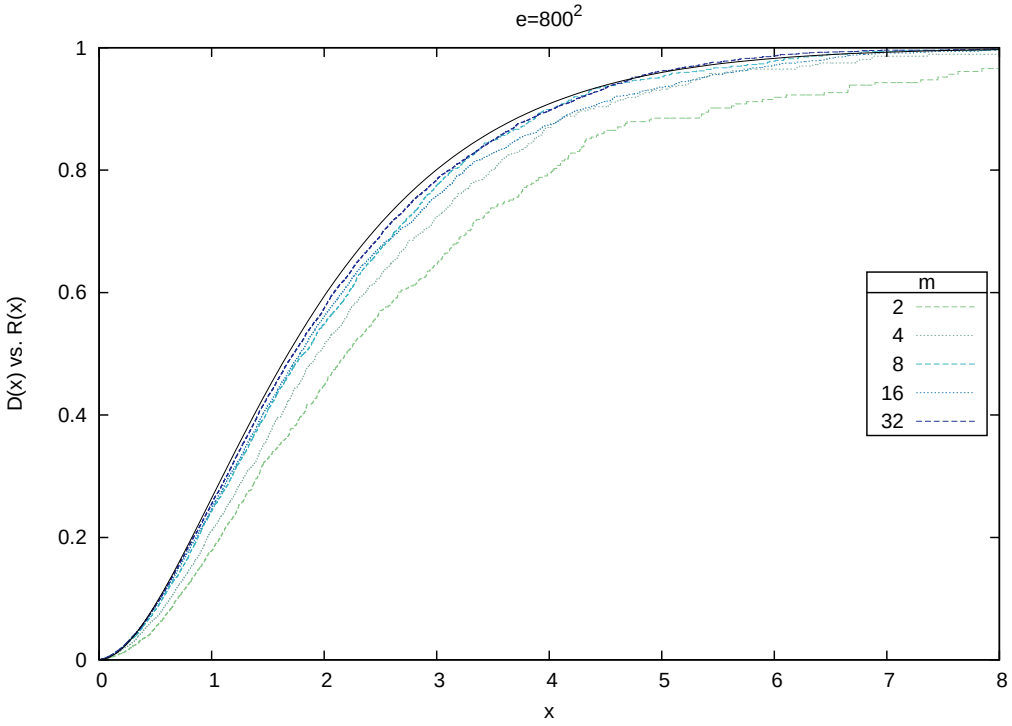

FIGURE 12. A number of the distributions $\mathscr{D}(x)$ calculated for $n = 800$ (green-blue dashed lines). The number m refers to the multiple of the characteristic length scale ρ^* sampled. The solid black line is the limiting distribution $\mathcal{R}(x)$.

For $e = n^2 \in \mathscr{E}$, we wish to calculate a sequence of period distribution functions, which will serve as approximations to $\mathscr{D}^e$ as $e \to \infty$. We calculate these period distribution functions over a sequence of Φ-invariant sets which mimic the fundamental domains defined in (55) —the natural invariant structures of the twist dynamics.

We consider subsets $A = A(e, m, \lambda)$ of X^e of the form

$$A(e, m, \lambda) = \{z \in X^e \,:\, \nu(z) \in [-1/2, m - 1/2]\} \qquad m \in \mathbb{N}. \tag{60}$$

For sufficiently small λ, the counterpart of A on the cylinder covers m copies of the fundamental domain of the twist dynamics, so that as $e \to \infty$:

$$\#A \sim 2m(2\langle e/2\rangle + 1)^2|\rho^*| \to \infty$$

(cf. equation (56)).

The set A is not invariant under the perturbed dynamics Φ. Hence we define $\bar{A}$ to be the smallest invariant set which contains A:

$$\bar{A}(e, m, \lambda) = \bigcup_{k\in\mathbb{Z}} \Phi^k(A(e, m, \lambda)).$$

The finiteness of the set $\bar{A}$ relies on the conjectured periodicity of all orbits (section 1).

We collect our findings as a series of observations. First, we observe that the overspill from A under the map Φ, i.e., the set $\bar{A} \setminus A$, is small relative to A as $m \to \infty$ (see figure 13(a)). On the basis of this observation, in what follows, it is assumed that there is a critical parameter value $\lambda_c(e, m)$ such that $\bar{A} \subset X^e$ for all $\lambda < \lambda_c$.

Observation 1. *Let $e = n^2 \in \mathscr{E}$. Then for a sequence (λ_m) of parameter values satisfying $\lambda_m < \lambda_c(n^2, m)$, we have:*

$$\frac{\#\bar{A}(n^2, m, \lambda_m)}{\#A(n^2, m, \lambda_m)} \to 1 \qquad m \to \infty.$$

Then we measure the period distribution function $\mathscr{D} = \mathscr{D}(n^2, m, \lambda)$ of Φ over $\bar{A}$:

$$\mathscr{D}(x) = \frac{\#\{z \in \bar{A} \,:\, \tau(z) \leqslant \gamma x\}}{\#\bar{A}},$$

where the scaling constant $\gamma = \gamma(n^2, m, \lambda)$ is given by

$$\gamma = \frac{2\#\bar{A}}{g+h} \qquad g = \#\left(\operatorname{Fix} G^e \cap \bar{A}\right) \qquad h = \#\left(\operatorname{Fix}(\Phi \circ G^e) \cap \bar{A}\right). \tag{61}$$

Assuming that the torus structure used to define $\mathscr{D}^e$ does not affect the period of the orbits, then, as $m \to \infty$, i.e., as we sample an increasing number of characteristic lengths ρ^*, the empirical period distribution approaches $\mathscr{D}^e$. As n increases, we need to ensure that m is large enough to achieve numerical convergence. In practice, small values of m were sufficient (see table 2).

Since $\operatorname{Fix} G^e$ is the pair of lines $x = y$ and $x - y = -\lambda(2\langle e/2\rangle + 1)$, the corresponding set on the cylinder is given by (cf. (54))

$$\eta^e(\operatorname{Fix} G^e) = \left\{ \frac{1}{2(2\langle e/2\rangle + 1)} (i, i + 2j) \,:\, i \in \{-(2\langle e/2\rangle + 1), 0\},\ j \in \mathbb{Z} \right\}.$$

Intersecting this with A (see equation (60)) restricts the index j according to

$$\frac{i + 2j}{2|\rho^*|(2\langle e/2\rangle + 1)} \in \left[-\frac{1}{2}, m - \frac{1}{2} \right).$$

Thus, equating A with $\bar{A}$ in the limit, we have

$$g \sim \#\left(\operatorname{Fix} G^e \cap A\right) \sim 2m|\rho^*|(2\langle e/2\rangle + 1) \to \infty$$

as $m, n \to \infty$. The fixed space $\operatorname{Fix}(\Phi \circ G^e)$ is the lattice equivalent of the line $\operatorname{Fix} H^e$ of equation (34). We have the following experimental observation for the size of h (see figure 13(b)).

Observation 2. *Let $e = n^2 \in \mathscr{E}$. Then for a sequence $(\lambda_{n,m})$ of parameter values satisfying $\lambda_{n,m} < \lambda_c(n^2, m)$, we have:*

$$h \sim \frac{g}{\sqrt{2}} \qquad m, n \to \infty.$$

From this observation, it follows that

$$\frac{g+h}{\#\bar{A}} \sim \frac{(2+\sqrt{2})}{2(2\langle e/2\rangle + 1)} \to 0$$

as $m, n \to \infty$, and hence that the quantities g and h satisfy the conditions (59) of theorem 9. Indeed, we observe that the universal distribution $\mathcal{R}(x)$ is the limiting distribution for $\mathscr{D}$ in the limits $m, n \to \infty$ (see figure 12).

Observation 3. *With $e = n^2$ and $(\lambda_{n,m})$ as in observation 2, we have:*

$$\mathscr{D}(n^2, m, \lambda_{n,m}) \to \mathcal{R} \qquad m, n \to \infty,$$

where $\mathcal{R}$ is the universal distribution of equation (10).

Finally we note that, as in theorem 9, the symmetric orbits of Φ have full density (see figure 14).

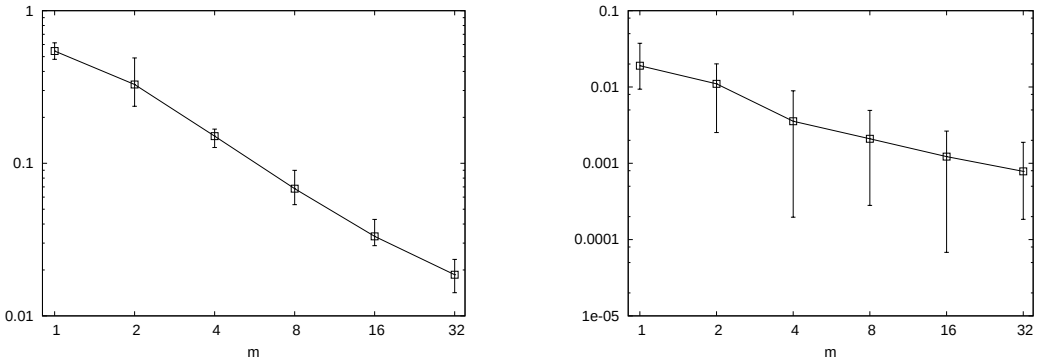

(a) $\#\bar{A}/\#A - 1$ (b) $h/g - 1/\sqrt{2}$

FIGURE 13. The convergence (a) of the ratio $\#\bar{A}/\#A$ to 1 and (b) of the ratio h/g to $1/\sqrt{2}$ as m becomes large, for $\langle e \rangle = 800$. The line shows the average value of the relevant ratio among all experiments performed: the error bars indicate its minimum and maximum value. All axes are displayed with a logarithmic scale.

Observation 4. *Let $S = S(e, m, \lambda)$ be the set of points in $\bar{A}$ whose orbit under Φ is symmetric:*

$$S = \{z \in \bar{A} \,:\, \mathcal{O}(z) = G^e(\mathcal{O}(z))\}.$$

Furthermore, let $e = n^2$ and $(\lambda_{n,m})$ be as in observation 2. Then, asymptotically, S has full density in $\bar{A}(m)$:

$$\frac{\#S(n^2, m, \lambda_{n,m})}{\#\bar{A}(n^2, m, \lambda_{n,m})} \to 1 \qquad m, n \to \infty.$$

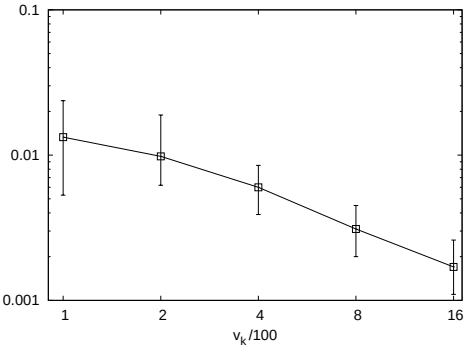

FIGURE 14. The quantity $1 - \#S/\#\bar{A}$ as $\langle e \rangle = n$ becomes large. The line shows the average value of the relevant ratio over all experiments performed (including over $m = 1, 2, 4, 8, 16, 32$—unlike the distribution $\mathscr{D}$ of figure 12, this ratio does not vary significantly with m): the error bars indicate its minimum and maximum value. The axes are displayed with a logarithmic scale.

Acknowledgements

We thank John A. G. Roberts for useful discussion. HRB thanks the School of Mathematics and Statistics at the University of New South Wales, Sydney, for their hospitality while part of this work was carried out.

References

[ABPS06] S. Akiyama, H. Brunotte, A. Pethő, and W. Steiner. Remarks on a conjecture on certain integer sequences. *Periodica Math. Hungarica*, 52:1–17, 2006.

[ABPS08] S. Akiyama, H. Brunotte, A. Pethő, and W. Steiner. Periodicity of certain piecewise affine integer sequences. *Tsukuba J. Math.*, 32:197–251, 2008.

[ABPT06] S. Akiyama, H. Brunotte, A. Pethő, and J. M. Thuswaldner. Generalized radix representations and dynamical systems II. *Acta Arith.*, 121:21–61, 2006.

[AP13] S. Akiyama and A. Pethő. Discretized rotation has infinitely many periodic orbits. *Nonlinearity*, 26:871–880, 2013.

[BV00] D. Bosio and F. Vivaldi. Round-off errors and p-adic numbers. *Nonlinearity*, 13:309–322, 2000.

[dFH13] J.A. de Faria and B. Hutz. Combinatorics of cycle lengths on Wehler K3 surfaces over finite fields. arXiv:1309.6598, 2013.

[Iwa05] M. Iwao. Analysis of ultradiscrete hamiltonian systems with lattice polygons. *J. Phys. Soc. Japan*, 74:3167–3178, 2005.

[KLV02] K.L. Kouptsov, J.H. Lowenstein, and F. Vivaldi. Quadratic rational rotations of the torus and dual lattice maps. *Nonlinearity*, 15:1795–1482, 2002.

[LHV97] J.H. Lowenstein, S. Hatjispyros, and F. Vivaldi. Quasi-periodicity, global stability and scaling in a model of Hamiltonian round-off. *Chaos*, 7:49–66, 1997.

[LV98] J.H. Lowenstein and F. Vivaldi. Anomalous transport in a model of Hamiltonian round-off. *Nonlinearity*, 11:1321–1350, 1998.

[LV00] J.H. Lowenstein and F. Vivaldi. Embedding dynamics for round-off errors near a periodic orbit. *Chaos*, 10:747–755, 2000.

[Nob08] A. Nobe. Ultradiscrete QRT maps and tropical elliptic curves. *J. Phys. A*, 41:125205 (12pp), 2008.

[NRV12] N. Neumärker, J.A.G. Roberts, and F. Vivaldi. Distribution of periodic orbits for the Casati-Prosen map on rational lattices. *Physica D*, 241:360–371, 2012.

[RB14] H. Reeve-Black. *Near-Integrable behaviour in a family of discretized rotations*. PhD thesis, Queen Mary, University of London, 2014.

[RBV13] H. Reeve-Black and F. Vivaldi. Near-integrable behaviour in a family of discretized rotations. *Nonlinearity*, 26:1227–1270, 2013.

[RV05] J.A.G. Roberts and F. Vivaldi. Signature of time-reversal symmetry in polynomial automorphisms over finite fields. *Nonlinearity*, 18:2171–2192, 2005.

[RV09] J.A.G. Roberts and F. Vivaldi. A combinatorial model for reversible rational maps over finite fields. *Nonlinearity*, 22:1965–1982, 2009.

[Sch11] R.E. Schwartz. Outer billiards and the pinwheel map. *J. Mod. Dyn.*, 5:255–283, 2011.

[Tab95] S. Tabachnikov. On the dual billiard problem. *Advances in Math.*, 115:221–249, 1995.

[Viv94] F. Vivaldi. Periodicity and transport from round-off errors. *Exp. Math.*, 3:303–315, 1994.

[Viv06] F. Vivaldi. The arithmetic of discretised rotations. In *AIP Conf. Proc.*, volume 826, pages 162–173, 2006.

[VV03] F. Vivaldi and I. Vladimirov. Pseudo-randomness of round-off errors in discretized linear maps on the plane. *Int. J. of Bifurcations and Chaos*, 13:3373–3393, 2003.

School of Mathematical Sciences, Queen Mary, University of London, London E1 4NS, UK
E-mail address: h.reeve-black@qmul.ac.uk
E-mail address: f.vivaldi@qmul.ac.uk